ISSN 2523-6830

Volume 6, Issue 15 — July — December - 2022

Journal Innovative Design

ECORFAN®

Journal Innovative Design, Volume 6, Issue 15, July - December 2022, is a journal edited six monthly by ECORFAN-Taiwan. Taiwan, Taipei. YongHe district, ZhongXin, Street 69. Postcode: 23445. WEB: www.ecorfan.org/taiwan, revista@ecorfan.org. Chief Editor: CAMPOS - QUIROGA, Peter. PhD. ISSN-On line: 2523-6830. Responsible for the latest update of this number ECORFAN Computer Unit. ESCAMILLA-BOUCHÁN, Imelda, PhD, LUNA-SOTO, Vladimir. PhD. Taiwan, Taipei. YongHe district, ZhongXin, Street 69, last updated December 31, 2022.

Journal Innovative Design

Scientific Objectives

Support the international scientific community in its written production Science, Technology and Innovation in the Field of Engineering and Technology, in Subdisciplines Design, Mechanical design, Electrical, Economic engineering, Technological innovation, Operations research, Solid waste management and treatments, Manufacturing, Planning, Industrial planning, Production, Programming and manufacturing, Industrial safety, Systems.

ECORFAN-Mexico SC is a Scientific and Technological Company in contribution to the Human Resource training focused on the continuity in the critical analysis of International Research and is attached to CONACYT-RENIECYT number 1702902, its commitment is to disseminate research and contributions of the International Scientific Community, academic institutions, agencies and entities of the public and private sectors and contribute to the linking of researchers who carry out scientific activities, technological developments and training of specialized human resources with governments, companies and social organizations.

Encourage the interlocution of the International Scientific Community with other Study Centers in Mexico and abroad and promote a wide incorporation of academics, specialists and researchers to the publication in Science Structures of Autonomous Universities - State Public Universities - Federal IES - Polytechnic Universities - Technological Universities - Federal Technological Institutes - Normal Schools - Decentralized Technological Institutes - Intercultural Universities - S & T Councils - CONACYT Research Centers.

Scope, Coverage and Audience

Journal Innovative Design is a Research Journal edited by ECORFAN-Mexico S.C in its Holding with repository in Taiwan, is a scientific publication arbitrated and indexed with semester periods. It supports a wide range of contents that are evaluated by academic peers by the Double-Blind method, around subjects related to the theory and practice of Design, Mechanical design, Electrical, Economic engineering, Technological innovation, Operations research, Solid waste management and treatments, Manufacturing, Planning, Industrial planning, Production, Programming and manufacturing, Industrial safety, Systems with diverse approaches and perspectives, That contribute to the diffusion of the development of Science Technology and Innovation that allow the arguments related to the decision making and influence in the formulation of international policies in the Field of Engineering and Technology. The editorial horizon of ECORFAN-Mexico® extends beyond the academy and integrates other segments of research and analysis outside the scope, as long as they meet the requirements of rigorous argumentative and scientific, as well as addressing issues of general and current interest of the International Scientific Society.

Editorial Board

Arbitration Committee

Assignment of Rights

The sending of an Article to Journal Innovative Design emanates the commitment of the author not to submit it simultaneously to the consideration of other series publications for it must complement the Originality Format for its Article.

The authors sign the Authorization Format for their Article to be disseminated by means that ECORFAN-Mexico, S.C. In its Holding Taiwan considers pertinent for disclosure and diffusion of its Article its Rights of Work.

Declaration of Authorship

Indicate the Name of Author and Coauthors at most in the participation of the Article and indicate in extensive the Institutional Affiliation indicating the Department.

Identify the Name of Author and Coauthors at most with the CVU Scholarship Number-PNPC or SNI-CONACYT- Indicating the Researcher Level and their Google Scholar Profile to verify their Citation Level and H index.

Identify the Name of Author and Coauthors at most in the Science and Technology Profiles widely accepted by the International Scientific Community ORC ID - Researcher ID Thomson - arXiv Author ID - PubMed Author ID - Open ID respectively.

Indicate the contact for correspondence to the Author (Mail and Telephone) and indicate the Researcher who contributes as the first Author of the Article.

Plagiarism Detection

All Articles will be tested by plagiarism software PLAGSCAN if a plagiarism level is detected Positive will not be sent to arbitration and will be rescinded of the reception of the Article notifying the Authors responsible, claiming that academic plagiarism is criminalized in the Penal Code.

Arbitration Process

All Articles will be evaluated by academic peers by the Double Blind method, the Arbitration Approval is a requirement for the Editorial Board to make a final decision that will be final in all cases. MARVID® is a derivative brand of ECORFAN® specialized in providing the expert evaluators all of them with Doctorate degree and distinction of International Researchers in the respective Councils of Science and Technology the counterpart of CONACYT for the chapters of America-Europe-Asia-Africa and Oceania. The identification of the authorship should only appear on a first removable page, in order to ensure that the Arbitration process is anonymous and covers the following stages: Identification of the Research Journal with its author occupation rate - Identification of Authors and Coauthors - Detection of plagiarism PLAGSCAN - Review of Formats of Authorization and Originality-Allocation to the Editorial Board- Allocation of the pair of Expert Arbitrators-Notification of Arbitration -Declaration of observations to the Author-Verification of Article Modified for Editing-Publication.

Instructions for Scientific, Technological and Innovation Publication

Knowledge Area

The works must be unpublished and refer to topics of Design, Mechanical design, Electrical, Economic engineering, Technological innovation, Operations research, Solid waste management and treatments, Manufacturing, Planning, Industrial planning, Production, Programming and manufacturing, Industrial safety, Systems and other topics related to Engineering and Technology.

Presentation of the content

In the first article we present, *Control based on GLRT algorithm for Unmanned Aerial Vehicle* by ZAVALA-CONTRERAS, Francisco Javier, ALAZKI, Hussain, CORTES-VEGA, David and GOLIKOV, Victor, with adscription in the Universidad Autónoma del Carmen, in the next article we present, *Neural Sliding mode control of a regenerative braking system for electric vehicles*, by RUZ-CANUL, Mario Antonio, DJILALI, Larbi, RUZ-HERNANDEZ, José Antonio and SANCHEZ-CAMPEROS, Edgar Nelson, with adscription in the Universidad Autónoma del Carmen, in the next article we present, *MAC-based Artificial Neural network for voice command recognition* by RODRÍGUEZ-PONCE, Rafael, with adscription in the Universidad Politécnica de Guanajuato, in the last article we present, *Spur gears with contact ratio less than unity*, by JIMÉNEZ-RABIELA, Homero, VÁZQUEZ-GONZÁLEZ, Benjamín, RAMÍREZ-CRUZ, José Luis and BRAVO-ACOSTA, Adrian Gustavo, with adscription in the Universidad Autónoma Metropolitana.

Content

Article **Journal Innovative Design**
December, 2022 Vol.6 No.15 1-9

Control based on GLRT algorithm for Unmanned Aerial Vehicle

Control basado en algoritmo GLRT para vehículos aéreos no tripulados

ZAVALA-CONTRERAS, Francisco Javier†, ALAZKI, Hussain, CORTES-VEGA, David* and GOLIKOV, Victor

Universidad Autónoma del Carmen Facultad de ingeniería

ID 1st Author: *Francisco Javier, Zavala-Contreras* /**ORC ID**: 0000-0003-2955-4827, **CVU CONACYT ID**: 1085721

ID 1st Co-author: *Hussain, Alazki* /**ORC ID**: 0000-0002-1960-3624

ID 2nd Co-author: *David, Cortés-Vega* /**ORC ID**: 0000-0002-6209-2081

ID 3rd Co-author: *Victor, Golikov* /**ORC ID**: 0000-0001-7909-9215

DOI: 10.35429/JID.2022.15.6.1.9 Received July 23, 2022; Accepted October 30, 2022

Abstract

This paper proposes the study of a vision-based control scheme for an Unmanned Aerial Vehicle (UAV) for tracking objects floating on the sea surface. The applied vision scheme is based on the generalized likelihood ratio test (GLRT) algorithm. Once the target is detected, its coordinates are computed and used by the UAV control to track the target. The quadrotor mathematical model is developed using the Newton-Euler approach and a PID controller is implemented to track the vector containing the coordinates obtained through the vision scheme. To verify the effectiveness of the proposal, simulation tests are developed in MATLAB/Simulink based on a real video of an objective floating in the sea surface. The obtained results show an appropriate detection and tracking of the objective.

Unmanned Aerial Vehicle, tracking control, GLRT

Resumen

En este artículo se propone el estudio de un esquema de control basado en visión para un Vehículo Aéreo No Tripulado (VANT) para el seguimiento de objetos flotantes sobre la superficie del mar. El esquema de visión aplicado está basado en la prueba de verisimilitud generalizada. Una vez que el objetivo es detectado, sus coordenadas son computarizadas y usadas por el control del VANT para realizar el seguimiento del objetivo. El modelo matemático del cuadrotor es desarrollado usando la aproximación Newton-Euler y el control PID es implementado para seguir el vector que contiene las coordenadas obtenidas a través del esquema de visión. Para verificar la efectividad de la propuesta, pruebas de simulación son desarrolladas en MATLAB/Simulink basándose en un video real de un objetivo flotando sobre la superficie del mar. Los resultados obtenidos muestran una detección y seguimientos apropiados del objetivo.

Vehículos Aéreos No Tripulados, Control de seguimiento, Prueba de verisimilitud generalizada

Citation: ZAVALA-CONTRERAS, Francisco Javier, ALAZKI, Hussain, CORTES-VEGA, David and GOLIKOV, Victor. Control based on GLRT algorithm for Unmanned Aerial Vehicle. Journal Innovative Design. 2022, 6-15: 1-9

*Author's Correspondence (email: dcortes@pampano.unacar.mx)
†Researcher contributing as first author.

I. Introduction

The Unmanned Aerial Vehicles (UAV) are versatile tools used to perform several tasks where a human pilot is not desirable. Nowadays, applications in which UAVs are useful are everywhere. In [1], a UAV is used to support the inspection and planning of building construction by giving a better view of the ground conditions, while an obstacle avoidance control was also applied to make the workflow faster. UAVs are also used for data acquisition after a natural disaster, monitoring the development of a city's infrastructure and environmental management as shown in [2]. In [3] a UAV is used for 3D mapping and monitoring tasks of an ecosystem located in Antarctica. To optimize pesticides application over plantations, in [4] a wireless sensor network was installed on a plantation to send relevant information to a UAV that be responsible for controlling the spreading process reducing deviations caused by wind.

Normally when UAVs are used for a specific task, they are controlled remotely by an operator on the ground, or they use sensors to locate themselves such as GPS or an ultrasonic sensor to detect the height at which they fly. However, many times they integrate a camera with which they obtain information to perform mapping or data collection. Some works have been performed where a camera is incorporated in the UAV as a sensor to obtain precise information about its own location, or the location of an object on which trajectory tracking can be performed based on the information collected by the camera. An example of such use of the camera is presented in [5] for the inspection of pipelines carrying gasoline and oil, where a UAV equipped with a non-contact sensor that perform external inspections of the pipes is proposed. The camera is pointing downwards to detect if the pipelines are aligned with the trajectory of the UAV, while a PID controller is responsible for maintaining the angles of the pipe and the desired trajectory.

The algorithms applied to computational vision arise from the necessity of object detection in dangerous environments for humans. One of them is [6], where a vision system is implemented to detect sea mines that were left on the surface of the ocean and avoid them.

In [7] a vision-based control for a UAV monitoring a bridge within an unknown 3D environment is presented, an adaptive nonlinear tracking control law is proposed together with a homography matrix computed from the visual information which allows the effective tracking and depth estimation. The depth estimation is useful for an approximation of the desired distance separating the camera from the target. An application of a computational vision system for a landing maneuver is shown in [8], where the camera detects a landmark by means of contour detection, image thresholding, and other mathematical techniques, obtaining fast, simple, and robust results. In [9] a computer vision system is developed based on an algorithm for landmark detection and tracking, which estimates the UAV motion (position and linear velocity) relative to a landing pad on the ground, the algorithm creates a homography matrix H for each view of the landing pad circles, calculating the height at which the UAV is located.

The work [10] presents an algorithm based on the Generalized Likelihood Ratio Test (GLRT) called Adaptive Subspace Detector (ASD) which aims to detect an object floating in the sea without knowing a priori its size, shape, and position in a sequence of images using optical sensors and infrared devices, the quality of detection is not affected by low contrast or background noise, so it is a viable option for detecting objects. In [11] the ASD and Modified Adaptive Subspace Detector (MASD) algorithms are implemented in some videos collected by a quadrotor with a camera pointing downwards. The videos are analyzed and some parameters such as the window size, the number of harmonics, and the number of frames analyzed are changed to perform a comparison of which algorithm works better under certain conditions.

There are several techniques for the control of UAVs like PID, Feedback linearization, Linear Quadratic Regulation (LQR), Sliding mode, Backstepping among others. The PID has a straightforward structure that is simple to build, offers high performance and a simple parameter's tuning process, is not typically used in underactuated systems but can be adapted to do it, also PID control does not consider the gyroscope effect and ignores air friction too [12].

ISSN-2523-6830

The LQR controller can be designed to obtain robust characteristics against disturbances, the stability of the system depends on the correct tuning parameter of the gain matrix K, but more complex calculus must be done. A comparison between PID and LQR is presented in [13], where the ease of implementation of PID controllers stands out over LQR schemes.

Hence this paper proposes the development of a vision-based control system for a quadrotor vehicle using GLRT algorithm to detect an objective floating in the sea surface in every video frame and compute its corresponding trajectory, with a PID controller to track such trajectory.

The remainder of this paper is organized as follows: Section II presents the mathematical model of the quadrotor. Section III presents information related to GLRT vision algorithm operation. Section IV shows a description of the proposed system and section V summarizes the results obtained from the simulation. Finally, section VI presents the conclusions of the work.

II. UAV Mathematical Model

The body of the quadrotor is constituted by 2 bars joined perpendicularly at the center of mass has 4 motors one for each end, the direction of rotation of the motors it's important because if they all spin in the same direction the UAV would start to revolve on *z*-axis that's why the motors must rotate like Figure 1.

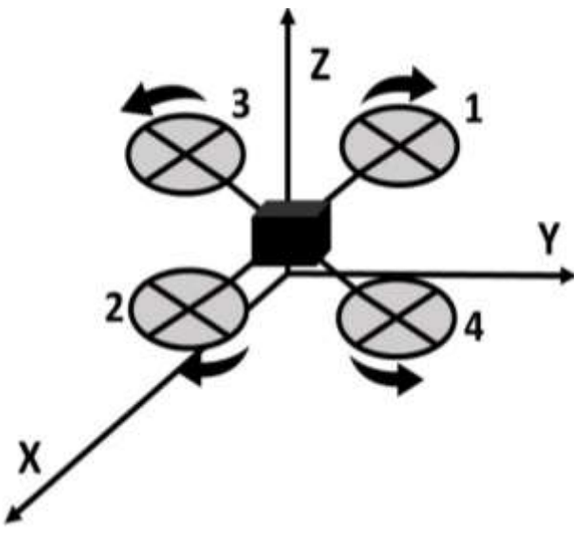

Figure 1 UAV motors alignment

The quadrotor is considered as a solid body and to describe its motion it is necessary to establish 2 reference systems, the first one is fixed to the ground denoted as a vector called J_F for inertial frame equal to:

$$J_F = \{\vec{x}\vec{y}\vec{z}\} \tag{1}$$

The second is associated with the center of mass and is the one that delimits the motion of the quadrotor for the inertial reference system is denoted as F_B:

$$F_B = \{\vec{x}_L\vec{y}_L\vec{z}_L\} \tag{2}$$

From these 2 reference systems it is possible to know the linear and angular position of the UAV. The linear position, the linear velocity and the angular position are described as follows [14]:

$$\xi = [x, y, z]^T \in \mathbb{R}^3 \tag{3}$$

$$\dot{\xi} = v \tag{4}$$

The UAV body can rotate about its center of mass in the 3 axes of the reference frame shown in (2) by the acceleration or deceleration of its four motors, for example, taking into account the organization of the Figure 1 we can say that if we increase the speed of motor 3 and decrease the speed of motor 4 the UAV will rotate on the *x*-axis to the right if we take motor 1 as a front, on the other hand, this rotation can be represented by the rotation matrix on the *x*-axis described below.

$$\begin{bmatrix} x_1 \\ y_1 \\ z_1 \end{bmatrix} = \begin{bmatrix} 1 & 0 & 0 \\ 0 & cos\phi & sin\phi \\ 0 & -sin\phi & cos\phi \end{bmatrix} \begin{bmatrix} x_2 \\ y_2 \\ z_2 \end{bmatrix} \tag{5}$$

where ϕ is a Euler angle for the *x*-axis commonly called Roll.

Furthermore, under the same dynamics, decreasing the power of motor 1 and increasing the power of motor 2 will cause a rotation, but in the *y*-axis with its corresponding rotation matrix:

$$\begin{bmatrix} x_1 \\ y_1 \\ z_1 \end{bmatrix} = \begin{bmatrix} cos\theta & 0 & sin\theta \\ 0 & 1 & 0 \\ -sin\theta & 0 & cos\theta \end{bmatrix} \begin{bmatrix} x_2 \\ y_2 \\ z_2 \end{bmatrix} \tag{6}$$

where θ is Euler angle for the *y*-axis called Pitch

In this case, increasing the power of motors 1 and 2 would cause rotation in the UAV over the *z*-axis clockwise, otherwise, increasing the power of motors 3 and 4 would cause rotation in the UAV counterclockwise over the *z*-axis, the rotation matrix is shown below:

$$\begin{bmatrix} x_1 \\ y_1 \\ z_1 \end{bmatrix} = \begin{bmatrix} cos\psi & -sin\psi & 0 \\ sin\psi & cos\psi & 0 \\ 0 & 0 & 1 \end{bmatrix} \begin{bmatrix} x_2 \\ y_2 \\ z_2 \end{bmatrix} \quad (7)$$

where ψ is Euler angle for the *z*-axis called Yaw. By multiplying the three matrices it is possible to constitute the rotation matrix of F_B that will give the position of the rigid body for the inertial frame this matrix it is called the cosine matrix[15]:

$$R_I = \begin{pmatrix} C\psi C\theta & C\psi S\phi S\theta - C\phi S\psi & S\phi S\psi + C\phi C\psi S\theta \\ C\theta S\psi & C\phi C\psi + S\phi S\psi S\theta & C\phi S\psi S\theta - C\psi S\phi \\ -S\theta & C\theta S\phi & C\phi C\theta \end{pmatrix} \quad (8)$$

where $C(*)$ stands for cosine and $S(*)$ for sinus. The dynamics of the system is divided in 2 main parts the translational and the orientation, where the first 3 equations are fully based on Newton's second law and describe translational motion based on the direction cosine matrix and multiplies the force shown below:

$$m \begin{bmatrix} \ddot{x} \\ \ddot{y} \\ \ddot{z} \end{bmatrix} + mg \begin{bmatrix} 0 \\ 0 \\ 1 \end{bmatrix} = R_I F \quad (9)$$

Where m is mass and g is the gravity form this multiplication is derived from the next three equations describing the lineal movement of the UAV:

$$\ddot{x} = \frac{1}{m}(\cos\psi sin\theta cos\phi + \sin\psi \sin\phi)\frac{U_1}{m} \quad (10)$$

$$\ddot{y} = \frac{1}{m}(\sin\psi sin\theta cos\phi + \cos\psi \sin\phi)\frac{U_1}{m} \quad (11)$$

$$\ddot{z} = -g + \frac{1}{m}(cos\ \theta cos\phi)\frac{U_1}{m} \quad (12)$$

where U_1 is the principal control signal of the 4 motors.

On the other hand, the second part of the model is the orientational system with three equations describing the angular movement of the UAV. The angular position vector and the angular velocity vector are described by:

$$\eta = [\phi, \theta, \psi]^T \quad (13)$$

$$\omega = [p\ q\ r]^T \quad (14)$$

where η is the angular position vector, $p\ q$ and r the angular velocity of the UAV for the *x*, *y* and *z*-axis The total kinetic energy of the system as a function of generalized coordinates of η is expressed as:

$$E_{cR} = \frac{1}{2}\dot{\eta}^T J(\eta)\dot{\eta} \quad (15)$$

where $J(\eta)$ is the Jacobian matrix defined as:

$$J(\eta) = W_\eta^T I W_\eta \quad (16)$$

the relationship between ω and $\dot{\eta}$ is given through the Jacobian W_η which is represented by the matrix

$$W_\eta = \begin{bmatrix} 1 & 0 & -sin\theta \\ 0 & cos\phi & cos\theta sin\phi \\ 0 & -sin\phi & cos\theta cos\phi \end{bmatrix} \quad (17)$$

and the inertia matrix *I*

$$I = \begin{bmatrix} I_{xx} & 0 & 0 \\ 0 & I_{yy} & 0 \\ 0 & 0 & I_{zz} \end{bmatrix} \quad (18)$$

performing the multiplication of all the matrices, the matrix result is:

$$J_\eta = \begin{bmatrix} I_{xx} & 0 & -I_{xx}S\theta \\ 0 & I_{yy} & (I_{yy} - I_{xx})C\phi S\phi C\theta \\ -I_{xx}S\theta & (I_{yy} - I_{xx})C\phi S\phi C\theta & I_{xx}S^2\theta + I_{yy}S^2\phi C^2\theta + I_{zz}C^2\phi C^2\theta \end{bmatrix} \quad (19)$$

the rotational equations for the three axes are as follows:

$$\ddot{\phi} = \frac{(I_{xx}+I_{yy}-I_{zz})}{I_{xx}}\dot{\psi}\dot{\theta} + \frac{\tau_\phi}{I_{xx}} \quad (20)$$

$$\ddot{\theta} = \frac{(-I_{xx}-I_{yy}+I_{zz})}{I_{yy}}\dot{\psi}\dot{\phi} + \frac{\tau_\theta}{I_{yy}} \quad (21)$$

$$\ddot{\psi} = \frac{(I_{xx}-I_{yy}+I_{zz})}{I_{zz}}\dot{\phi}\dot{\theta} + \frac{\tau_\psi}{I_{zz}} \quad (22)$$

where I_{xx}, I_{yy} and I_{zz} are the moments of inertia in the *x*, *y*, and *z* axes.

III. GLRT algorithm

GLRT allows object detection even when the size, shape, and position are unknown using a sequence of images as input data. It is used like a universal detector for detection problems. There are two options for this kind of detector; if the target is present during a scan, it will return the signal target plus the signal from the background clutter; otherwise, if no target is present, it will return exclusively the background clutter. The basic premises for modeling a sequence of pixels are: 1) the background consists of several oscillating elements and 2) the target oscillates as a solid element [12]. It uses video spatial-temporal patches, called bricks, to determine whether the observed brick contains a target in the presence of a random background. A hypothesis test is made to distinguish a pixel with the signal of the target-plus noise (H_1) these pixels contain the target signal plus channel noise from the others who contain the background clutter plus channel noise.(H_0).Under H_0 we have:

$$x_j = \sigma_{0,j} n_j \tag{23}$$

where x_j are a real pixel-vectors, n_j is the noise pixel-vector and $\sigma_{0,j}$ is the variance of the background plus channel noise. Under H_1 is the signal plus background plus channel noise hypothesis is:

$$x_j = s_j + \sigma_{1,j} n_j \tag{24}$$

Where $s_j = H\theta_j$ is the deterministic signal of interest that belongs to a known subspace, H is an orthogonal target Vandermonde matrix:

$$H = \begin{bmatrix} 1 & 1 & \dots & 1 \\ Z_1 & Z_2 & \dots & Z_p \\ \vdots & \vdots & \dots & \vdots \\ Z_1^{K-1} & Z_2^{K-1} & \dots & Z_p^{K-1} \end{bmatrix} \tag{25}$$

Hence it is considered the problem of detecting an optical target in N digital images, assuming the target may be present completely or partially in the brick with size L of pixel vectors, Let $j = 1, \dots, U$ be a subset of integers indexing the pixel vectors (U is unknown) which may contain an unknown object under the H_1 hypothesis and $j = U + 1, \dots, L$ is the subset of the pixel-vectors, which do not contain the object under the H_1.

The secondary dataset consists of GL pixel vector$x_j, N \times 1, j = L + 1,2, \dots, (G + 1)L$ which are assumed to have the background clutter and white channel noise components only.

Then, the hypotheses can be expressed as:

$$\begin{cases} H_0: x_j = c_j + n_j, j = 1,2, \dots, (G+1)L \\ H_1: \begin{cases} x_j = s_j + n_j, j = 1, \dots, U \\ x_j = c_j + n_j, j = U+1, \dots, (G+1)L \end{cases} \end{cases} \tag{26}$$

IV. Vision-based control scheme

The proposed vision-based control scheme is illustrated in the block diagram in Figure 2.

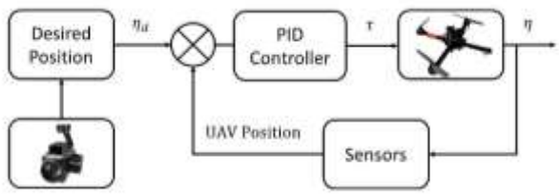

Figure 2 Block diagram of the proposed scheme

The PID-based control scheme uses 4 references to control the 6 degrees of freedom of the UAV movement as previously defined, 6 equations were developed to describes those movements.

The mathematical model is inserted in Simulink allowing the simulation of the system, the references are, the linear displacement in the *z*-axis, in which all the motors are used at the same time to lift the UAV body, and the control of the rotations in the 3 axes of the angular displacement on the body coordinate system. It is through these rotations that indirectly the body can move along the *x* and *y* axes linearly.

The PID control can follow trajectories in the *xy* plane under the consideration of a fixed height, so the *xy* plane can be related to the input images that also have two dimensions (height and width). The parameters used in the simulation for the model of the considered quadrotor are shown in Table 1.

ISSN-2523-6830

Parameter	Symbol	Value
Gravity	g	9.81 m/s^2
Mass	m	0.468 kg
Length of arm	l	0.225 m
Drag constant	d	2.98e-6 $N*m*s^2$
Thrust constant	b	2.930e-6 N*s^2
Rotor inertia	J_r	3.335e-5 $kg*m^2$
Inertia in *x*-axis	I_{xx}	4.856e-3 $kg*m^2$
Inertia in *y*-axis	I_{yy}	4.856e-3 $kg*m^2$
Inertia in *z*-axis	I_{zz}	8.801e-3 $kg*m^2$

Table 1 Values form the mathematical model

The vision algorithm uses images obtained from a camera mounted inside the body of the UAV. After obtaining these images analyzes a set of these, within each image there are two types of frame, a detection frame and a frame that is responsible for collecting data to generate the threshold that determines whether the target is present or not, the frame that generates the threshold is a square of 10 pixels by 10 pixels, while the detection region is selected as a frame where the object is intended to be detect, a sample of 50 images where the target was detected in various positions was taken.

As the image is an array of pixels in two dimensions, the pixels can be taken as units of a cartesian plane and the pixels in which the target was detected become points that can be located with 2 numbers expressed in coordinates, these coordinates have their point of origin in the lower left corner. Once the coordinates of the points along the 50 images are collected, it is possible to transform these data into elements of a vector of positions that will generate a trajectory. Such trajectory is used as the reference to be tracked by the quadrotor using a PID-based control scheme.

V- Results

In order to validate the viability of the proposal a simulation test has been developed in Matlab/Simulink. The objective detection and trajectory generation are performed on a video taken from a quadrotor with a mounted camera. This video shows a person, which is the objective to detect, swimming in the sea's surface with some waves as illustrated in Figure 3.

Figure 3 Objective in one frame of the video

Once the objective is detected the algorithm computes its trajectories and send them to the quadrotor to perform its tracking. The tracking process is based on PD controllers in cascade for the *x* and *y* axes, while a direct loop is used for the *z* axis like it's shown in the Figure 4.

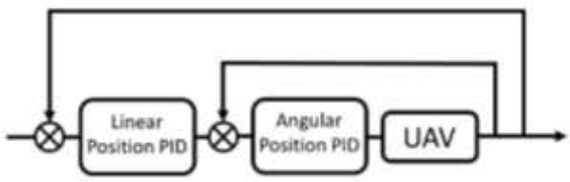

Figure 4 Controller PD in cascade

The corresponding parameters of these controllers are shown in Table 2.

Controller	P	I	D
Linear Position loop (*x*-axis)	1	/	0.5
Linear Position loop (*y*-axis)	1	/	0.5
Linear Position loop (*z*-axis)	5	/	8
Angular Position loop (*x*-axis)	1	10	1
Angular Position loop (*y*-axis)	1	10	1

Table 2 PID controller parameters

The objective of the proposed vision-based control scheme is to keep this target within the camera range, ensuring that the target is under the UAV. The trajectories obtained from the vision algorithm were introduced as the desired reference positions into the mathematic model of the quadrotor to perform the trajectory tracking stage.

ISSN-2523-6830

The height at which the video was taken is approximately 10 meters, so this is the desired value used for the *z*-axis. Since height is supposed constant the control objective is to maintain this value at every instant which is depicted in Figure 5.

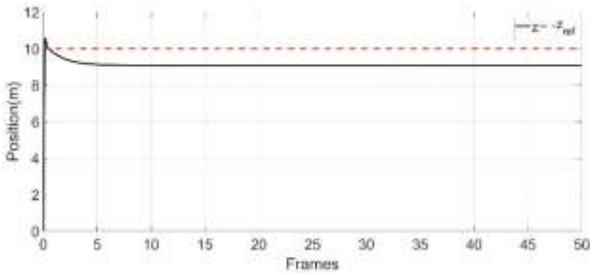

Figure 5 Desired and actual trajectories in *z*-axis

In another hand for the *x*-axis the path it is according to the coordinate of the image width this parameter allows to the PID controller to follow the target across all the *xy* plane to keep it in the center of the image. In the Figure 5 the location of the target and the position of the UAV are shown, in the beginning they are separated but the PID controller acts to align the UAV's position with that of the detected object.

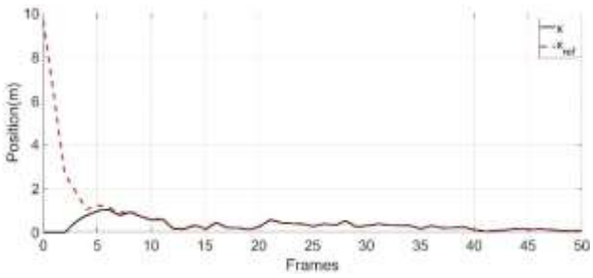

Figure 6 Desired and actual trajectories in *x*-axis

The desired and actual trajectories for the *y*-axis are shown in Figure 7. The object has low movement in this axis, so the trajectory shows small changes which are tracked with enough accuracy by the controller.

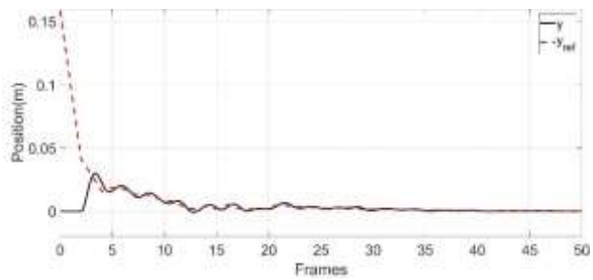

Figure 7 Desired and actual trajectories in *y*-axis

The tracking error for all axes is presented in Figure 8, where can be observed that the desired trajectory for the *x* and *y* axes is properly tracked with low error values. On the other hand, the controller for *z*-axis shows a greater steady state error which can be improved with a better tuning of controller gains.

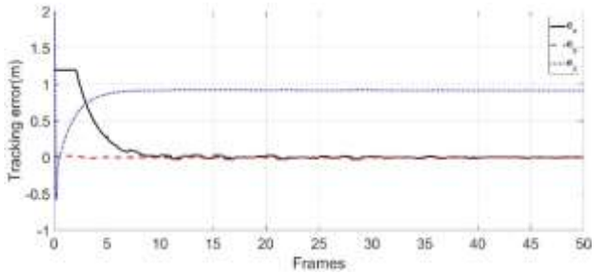

Figure 8 Tracking error (*x*-*y*-*z*-axis)

VI. Conclusions

This work presented the development of a vision-based control scheme for tracking objectives with a quadrotor equipped with a video camera. The GLRT algorithm is used to fulfill the detection task due to its robust features which allows the detection under unknown shape, size and position of the target. Once the detection is performed, the objective coordinates are computed to generate a trajectory to be tracked by a control scheme which ensures that the objective is inside the camera range. A PID control scheme is selected due to its simple tuning and implementation.

The results obtained show a good behavior of the detector, despite the constant oscillation generated by the sea waves, it managed to capture with sufficient accuracy the target within the image allowing the generation of the objective trajectory. The PID control was able to maintain an appropriated tracking of the given coordinates both in the *x* and *y* axis, however, the desired height was not reached remaining at 9 meters when the reference is 10. As future work an improvement in the control of the UAV can be done to maintain a correct altitude, as well as a real time application of the system to be tested in a disturbed environment.

Acknowledgements

To CONACYT and Universidad Autónoma del Carmen (UNACAR)

ISSN-2523-6830

Funding

This work has been funded by CONACYT [1085721] and Universidad Autónoma del Carmen (UNACAR) [153129]

References

[1] Freimuth, H., & König, M. (2018). Planning and executing construction inspections with unmanned aerial vehicles. Automation in Construction, 96, 540-553. https://doi.org/10.1016/j.autcon.2018.10.016

[2] Ezequiel, C. A. F., Cua, M., Libatique, N. C., Tangonan, G. L., Alampay, R., Labuguen, R. T., ... & Palma, B. (2014, May). UAV aerial imaging applications for post-disaster assessment, environmental management and infrastructure development. In 2014 International Conference on Unmanned Aircraft Systems (ICUAS) (pp. 274-283). IEEE. https://doi.org/10.1109/ICUAS.2014.6842266

[3] Lucieer, A., Turner, D., King, D. H., & Robinson, S. A. (2014). Using an Unmanned Aerial Vehicle (UAV) to capture micro-topography of Antarctic moss beds. International journal of applied earth observation and geoinformation, 27, 53-62. https://doi.org/10.1016/j.jag.2013.05.011

[4] Faiçal, B. S., Pessin, G., Geraldo Filho, P. R., Carvalho, A. C., Furquim, G., & Ueyama, J. (2014, November). Fine-tuning of UAV control rules for spraying pesticides on crop fields. In 2014 IEEE 26th International Conference on Tools with Artificial Intelligence (pp. 527-533). IEEE. https://doi.org/10.1109/ICTAI.2014.85

[5] Shukla, A., Xiaoqian, H., & Karki, H. (2016, October). Autonomous tracking of oil and gas pipelines by an unmanned aerial vehicle. In 2016 IEEE 59th International Midwest Symposium on Circuits and Systems (MWSCAS) (pp. 1-4). IEEE. https://doi.org/10.1109/MWSCAS.2016.7870114

[6] Borghgraef, A., Barnich, O., Lapierre, F., Van Droogenbroeck, M., Philips, W., & Acheroy, M. (2010). An evaluation of pixel-based methods for the detection of floating objects on the sea surface. EURASIP Journal on Advances in Signal Processing, 2010, 1-11. https://doi.org/10.1155/2010/978451

[7] Metni, N., Hamel, T., & Derkx, F. (2005, December). Visual tracking control of aerial robotic systems with adaptive depth estimation. In Proceedings of the 44th IEEE Conference on Decision and Control (pp. 6078-6084). IEEE. https://doi.org/10.1109/CDC.2005.1583134

[8] Vidal, V. F., Honório, L. M., Santos, M. F., Silva, M. F., Cerqueira, A. S., & Oliveira, E. J. (2017, May). UAV vision aided positioning system for location and landing. In 2017 18th international carpathian control conference (ICCC) (pp. 228-233). IEEE. https://doi.org/10.1109/CarpathianCC.2017.7970402

[9] Carrillo, L. R. G., Rondon, E., Sanchez, A., Dzul, A., & Lozano, R. (2010). Position control of a quad-rotor UAV using vision. IFAC Proceedings Volumes, 43(15), 31-36. https://doi.org/10.3182/20100906-5-JP-2022.00007

[10] Rodriguez-Blanco, M., & Golikov, V. (2016). Multiframe GLRT-based adaptive detection of multipixel targets on a sea surface. IEEE Journal of Selected Topics in Applied Earth Observations and Remote Sensing, 9(12), 5506-5512. https://doi.org/10.1109/JSTARS.2016.2582383

[11] Torres, L. S., Golikov, V., Zhilyakov, E., & Alazki, H. (2019, November). Target Detection On The Sea Surface Using a Quadrotor with a Video Camara. In 2019 IEEE International Autumn Meeting on Power, Electronics and Computing (ROPEC) (pp. 1-6). IEEE. https://doi.org/10.1109/ROPEC48299.2019.9057083

[12] Salih, A. L., Moghavvemi, M., Mohamed, H. A., & Gaeid, K. S. (2010). Flight PID controller design for a UAV quadrotor. Scientific research and essays, 5(23), 3660-3667. https://doi.org/10.5897/SRE.9000032

[13] Bouabdallah, S., Noth, A., & Siegwart, R. (2004, September). PID vs LQ control techniques applied to an indoor micro quadrotor. In 2004 IEEE/RSJ International Conference on Intelligent Robots and Systems (IROS)(IEEE Cat. No. 04CH37566) (Vol. 3, pp. 2451-2456). IEEE. https://doi.org/10.1109/IROS.2004.1389776

[14] Castillo, P., García, P., Lozano, R., & Albertos, P. (2007). Modelado y estabilización de un helicóptero con cuatro rotores. Revista Iberoamericana de Automática e Informática Industrial RIAI, 4(1), 41-57. https://doi.org/10.1016/S1697-7912(07)70191-7

[15] Chen, Y., He, Y., & Zhou, M. (2013). Modeling and control of a quadrotor helicopter system under impact of wind field. Research Journal of Applied Sciences, Engineering and Technology, 6(17), 3214-3221. http://dx.doi.org/10.19026/rjaset.6.3626

ISSN-2523-6830

Article **Journal Innovative Design**
June, 2022 Vol.6 No.15 10-18

Neural Sliding mode control of a regenerative braking system for electric vehicles

Control Neuronal por modos deslizantes para el frenado regenerativo de vehículos eléctricos

RUZ-CANUL, Mario Antonio†*, DJILALI, Larbi, RUZ-HERNANDEZ, José Antonio and SANCHEZ-CAMPEROS, Edgar Nelson

Universidad Autónoma del Carmen, Facultad de Ingeniería

ID 1st Author: *Mario Antonio, Ruz-Canul* / **ORC-ID:** 0000-0003-0872-062X, **CVU CONACYT ID**: 1085717

ID 1st Coauthor: *Larbi, Djilali* / **ORC-ID:** 0000-0002-3594-5747, **CVU CONACYT ID:** 696839

ID 2nd Coauthor: *José Antonio, Ruz-Hernández* / **ORC ID**: 0000-0001-8332-4980, **CVU CONACYT ID**: 216374

ID 3rd Coauthor: *Edgar Nelson, Sánchez-Camperos* /**ORC ID:** 0000-0002-8695-7879, **CVU CONACYT ID**: 597

DOI: 10.35429/JID.2022.15.6.10.18 Received July 23, 2022; Accepted October 30, 2022

Abstract

This paper summarizes the work done on the development of a Neural Sliding Mode Controller (NSMC) for a regenerative braking system used in an electric vehicle (EV), which is composed of a Main Energy System (MES) and an Auxiliary Energy System (AES). This last one contains a buck-boost converter and a super-capacitor. The AES aims to recover the energy generated during braking that the MES cannot retrieve and use later during acceleration. A neural identifier trained with the Extended Kalman Filter (EKF) has been used to estimate the buck-boost converter real dynamics and to build up the NSMC, which is implemented to regulate the voltage and current dynamics in the AES. Simulation results**,** illustrate the effectiveness of the proposed control scheme to track time-varying references of the AES voltage and current dynamics measured at the buck-boost converter and ensure the charging and discharging operation modes of the super-capacitor. In addition, the proposed control scheme enhances the EV storage system efficiency and performance, when the regenerative braking system is employed.

Regenerative Braking, Sliding Mode Controller, Electrical Vehicle.

Resumen

Este articulo recopila el trabajo realizado en el desarrollo de un Control por Modos Deslizantes Neuronal (NSMC) para el frenado regenerativo utilizado en un vehículo eléctrico, el cual está conformado por un Sistema Principal de Energía (MES) y un Sistema Auxiliar de Energía (AES). Este último contiene un convertidor elevador-reductor y un super capacitor. El objetivo del AES es recuperar la energía generada durante el frenado que el MES no puede recuperar y utilizarla después durante la aceleración. Un identificador neuronal entrenado con el Filtro de Kalman Extendido (EKF) ha sido utilizado para estimar las dinámicas reales del convertidor elevador-reductor y para diseñar el NSMC, el cual es implementado para regular el voltaje y la corriente en el AES. Los resultados de la simulación ilustran la efectividad del esquema de control propuesto para el seguimiento de referencias variables en el tiempo del voltaje y corriente del AES medidas en el convertidor elevador-reductor y el mejoramiento de los modos de operación de carga y descarga del super capacitor. Además, el esquema de control propuesto mejora la eficiencia y el rendimiento del sistema de almacenamiento del EV, cuando el sistema de frenado regenerativo es empleado.

Frenado regenerativo, Control por Modos Deslizantes, Vehículo Eléctrico

Citation: RUZ-CANUL, Mario Antonio, DJILALI, Larbi, RUZ-HERNANDEZ, José Antonio and SANCHEZ-CAMPEROS, Edgar Nelson. Neural Sliding mode control of a regenerative braking system for electric vehicles. Journal Innovative Design. 2022, 6-15: 10-18

*Correspondence to the Author (e-mail: 120664@mail.unacar.mx)
† Researcher contributing as first author.

I. Introduction

Nowadays, Electric Vehicles (EVs) present an important alternative solution to conventional vehicles, regarding gasoline prices, gas emissions, and climatic changes among other factors [1]. In EVs, electric motors can be controlled to be operated as generators to convert the kinetic or potential energy of vehicle mass into an electric one, which can be stored and utilized to improve the driving performance and extend the life of the storage system [2].

Different proposals have been developed to enhance the efficiency of EVs. One of the implemented solutions is called hybrid vehicles, which combine an internal combustion engine and an electric car motor improving the emission of exhaust gases over internal combustion vehicles [3]. Another type of hybrid vehicle has emerged, named the plug-in hybrid electric vehicle, which allows drivers to charge the battery bank using an external EV charger [4]. By using these technologies, various benefits can be achieved; however, the hybrid nature of these EVs required more complex hybrid controllers and communication systems to ensure the switching between both installed supply systems [5]. These challenges can be reduced by using fully-EVs technology using the combination of a Main Energy System (MES) and an Auxiliary Energy System (AES) based battery bank, super-capacitor, and power electronic devices, which provide an extended driving range, high power quality, regenerative braking capability, and better system efficiency [6].

Recently, the regenerative braking capability in EVs is one of the most important characteristics of EVs, which helps to recover energy during braking and enhances the storage system efficiency [7]. Different control methodologies and regenerative braking architectures have been investigated and implemented in the last years. In [8], a design of the regenerative braking for EV with help of an ultra-capacitor pack and battery is developed where the objective is to save the wasted energy during braking. Results illustrate that the additional super-capacitor pack improves the efficiency of the regenerative braking in comparison with the standalone battery system.

The same design is implemented in [9] where a Proportional-Integral (PI) controller is used to regulate the buck-boost converter output voltage related to the super-capacitor pack.

In [10] a fuzzy logic sliding mode controller is implemented using the exponential reaching law and parameter optimizing for an anti-lock braking system to keep the optimal slip value on the braking system of the EV. In [11] an intelligent sliding mode controller is employed to track the desired slip during a braking scenario; the obtained results illustrate a considerable energy recuperation without overcharging in the battery bank compared with the fuzzy sliding mode control developed in [10] and the Fuzzy one in [12].

Unfortunately, all controllers previously described required prior knowledge of system parameters, which are not always reachable in real cases. In addition, those control methodologies are not robust to disturbances, which affect system stability and system efficiency [13].

Regarding technology advances, complex unknown dynamics, and highly coupled behaviors are introduced, which force the control engineers to use appropriate mathematical tools to deal with control problems. Recently, Neural Networks (NNs) have been widely implemented in the approximation of unknown dynamics, then based on the obtained model, conventional controllers are developed. Different control problems are solved using neural control such as in multiagent stabilization systems [14], microgrids [15], biomedical applications [16], among others.

However, the EVs and regenerative braking system are less investigated using this neural control strategy [17]. This paper presents Neural Sliding Mode Controller (NSMC) for a regenerative braking system. The proposed controller is used to control the current and voltage of the buck-boost converter related to AES with the objective to recover the waste energy during braking and enhance the MES efficiency.

ISSN-2523-6830

The main contribution of the present paper is: 1) an online identification based Recurrent High Order Neural Network (RHONN) trained by the Extended Kalman Filter (EKF) is a build-up to approximate the DC buck-boost behaviors. 2) Based on the obtained neural model, the sliding mode is synthesized and implemented to track the buck-boost current and voltage desired dynamics. 3) since the proposed controller is based on the neural identifier, robustness to parameter variations and disturbances is ensured; in addition, chattering is significantly reduced on the tracked dynamics. 4) by the implementation of the proposed controller for the AES, the storage energy in MES is improved, moreover, energy lost is largely reduced in comparison with standalone MES. The paper is organized as follows: In section 2, the regenerative braking problem is described.

In section 3, mathematical preliminaries are introduced. In section 4, the system modeling, identification and control for the buck-boost converter are developed. In section 5, simulation results are presented.

Desarrollo de Secciones y Apartados del Artículo con numeración subsecuente

II. Regenerative Braking System

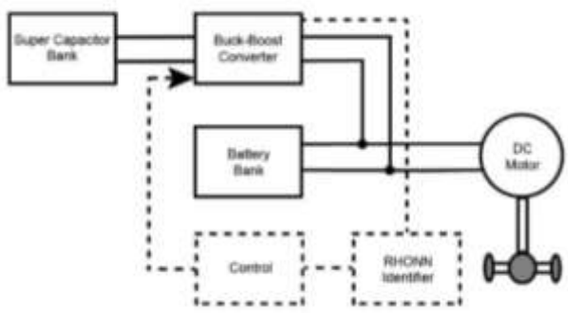

Figure 1 Regenerative Braking System

A regenerative braking system as depicted in Fig. 1 allows the recovery of kinetic energy produced during braking and its utilization to improve the energy storage efficiency and extend the operating distance of the EV [2]. This system is composed of a super-capacitor and buck-boost converter, which are part of the AES. In addition, a battery bank is used to administrate the energy to the electrical motor conforming to the MES.

The super-capacitor and the buck-boost converter are connected as illustrated in Fig. 2, with the objective of increasing or decreasing the output voltage depending on the following operation modes.

Buck operation

In this mode, the output voltage is decreased from the input voltage. To achieve such, T1 is OFF and T2 is activated, consequently, the energy is transferred from the capacitor (Vc) to the super-capacitor voltage (Vsc). When T2 is turned on, current flows from capacitor C, generating the Ic current to the super-capacitor. As the result, a fraction of this energy is charged into the inductance L. On the other hand, when T2 is turned off the current charged in L is discharged into Vc through the diode D1, driving the current in the direction of capacitor C [9].

Boost operation

On the other hand, in this mode, the output voltage is increased. To do such, T2 is deactivated and T1 is activated to transfer energy from the super-capacitors Vsc to the battery bank V c. When T1 is ON, the energy is acquired from the capacitor and stored in the inductance L.
Reversely, when T1 is OFF, the energy stored in the inductance is transferred into the capacitor through the diode D2 and keep it in the battery bank.

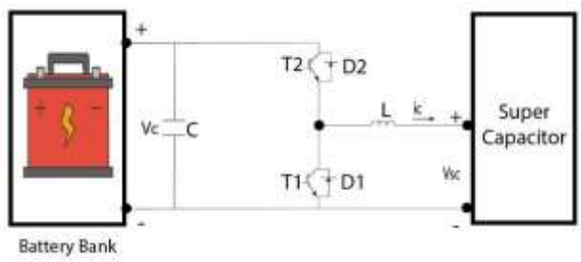

Figure 2 Buck-Boost Converter

During the braking operation, the brake manages the electricity generated by the motor into the batteries or capacitors. The DC-DC converter operates in boost function during acceleration while it operates into buck function in deceleration, which will make it easier in charging up the super-capacitor.

III. Mathematical Preliminaries

A. Discrete-Time Recurrent High Order Neural Networks

Recently, recurrent neural networks have been used in many applications and give excellent results in nonlinear dynamics approximations [13]. However, RHONN has demonstrated that is a good choice in nonlinear systems identification, which consists of adjusting the parameters of an appropriately selected model according to an adaptive law. Using a series-parallel configuration, the estimated state variable of a nonlinear system using the RHONN identifier is given by [18]

$$\chi_{i,k+1} = \omega_i^T \phi_i(x_k, u_k, k) \quad (1)$$

where $\chi_{i,k+1}$ is the state of the i^{th} neuron which identifies the i^{th}component of x_k, $x_k = [x_{1,k}, \dots, x_{n,k}]$is the state vector, $\omega_{i,k} \in \mathrm{R}^{L_i}$ are the adjustable synaptic weights of NNs, $u \in \mathrm{R}^m$ is the input vector, and $\phi_i(x_k, u_k, k) \in \mathrm{R}^{L_i}$is defined as [13].

$$\phi_i(x_k, u_k, k) = \begin{bmatrix} \phi_{i_1} \\ \phi_{i_k} \\ \vdots \\ \phi_{i_{L_i,k}} \end{bmatrix} = \begin{bmatrix} \prod_{j \in I_1} \zeta_{ij}^{d_{ij(1)}} \\ \prod_{j \in I_2} \zeta_{ij}^{d_{ij(2)}} \\ \vdots \\ \prod_{j \in I_{L_i}} \zeta_{ij}^{d_{ij(L_i)}} \end{bmatrix} \quad (2)$$

where $d_{ij,k}$are non-negative integers, L_i is the connection number, $I_1, I_2, \dots I_{L_i}$ is a non-ordered subset collection of $1,2 \dots, n+m$, n is the state dimension, m is the inputs dimension, and ζ_i is defined as [13].

$$\zeta_i = \begin{bmatrix} \zeta_{i_1} \\ \vdots \\ \zeta_{i_n} \\ \vdots \\ \zeta_{i_{n+m}} \end{bmatrix} = \begin{bmatrix} S(x_1) \\ \vdots \\ S_{x_n} \\ u_{1,k} \\ \vdots \\ u_{m,k} \end{bmatrix} \quad (3)$$

Where$u = [u_{1,k}, u_{2,k}, \dots, u_{m,k}^T]$ is the input vector to the network. The function $S(.)$ is a hyperbolic tangent function defined as

$$S(x_k) = \alpha_i \tanh(\beta_i x_k) \quad (4)$$

where x_k is the state variable; α and β are positive constants. To approximate a nonlinear model, the discrete-time RHONN in (1) is modified as [19].

$$\chi_{i,k+1} = \omega_i^T \phi_i(x_k) + \overline{\omega}_i^T \varphi_i(x_k, u_k) \quad (5)$$

where $\omega_{i,k}$ represents the adjustable weights, and $\overline{\omega}_{i,k}$ is fixed weights, φ_i is a linear function of the state vector or vector input u_k depending to the system structure or external inputs to the RHONN model. Fig. 3 illustrates an i^{th} RHONN identifier scheme.

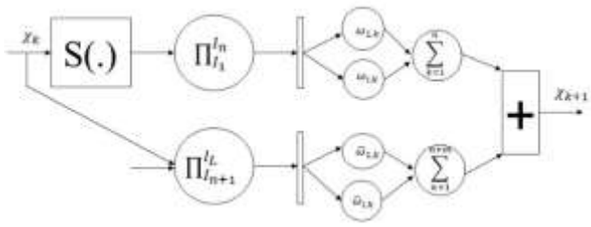

Figure 3 RHONN Scheme

B. Discrete-Time Sliding Mode Control

In the last decades, the sliding mode controller receives much attention due to its robustness to some class of perturbation. Consider the following nonlinear system [20]

$$\dot{x} = f(x, u, t) \quad (6)$$

with the bounded function $f(x)$, $|f(x)| < f_o =$ constant and the control law, as a relay function, which is used to track the error $e = r(t) - x$, $r(t)$ to zero where is the reference input, and u is defined as

$$u = \begin{cases} u_0 & if \quad s(x) \geq 0 \\ -u_0 & if \; s(x) < 0 \end{cases} \quad (7)$$

where $s(x)$ and u_0 are define as the sliding surface and the upper control bound, respectively.

Fig. 4 illustrates the behavior of the continuous-time system with scalar sliding mode control, where the state $x(t)$ initiates from an initial point $x(t=0)$, the trajectory reaches the sliding surface $S(x) = 0$ within finite time t_{sm} and remains on the surface subsequently.

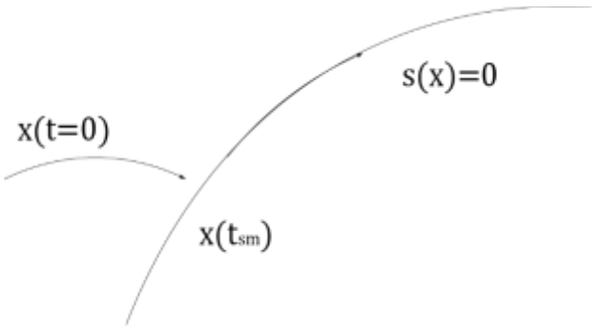

Figure 4 Motion trajectory of continuous system with scalar sliding mode control

When for each sampling point the function is derived $t_j = k\Delta t,\ k = 1,2\ldots$, the representation of the continuous time system in discrete time in (6) is

$$x_{k+1} = F(x_k) \tag{8}$$

with the condition that starting from t_{sm}, the trajectory belongs to the sliding manifold with $s(x(t))$, or for a $k_m \geq t_{sm}/\Delta t$ [20].

$$s(x_k) = 0 \qquad \forall k \geq k_{sm} \tag{9}$$

This motion can be defined as discrete time sliding mode. Consequently, from (6) and in scenario where for any constant control u and any initial condition $x(0)$, its solution can be written in closed form as [21].

$$x(t) = F(x(0), u) \tag{10}$$

with u_k should be selected at each sampling point k such that this constant control signal will achieve $s(x_{k+1})$. The discrete-time system is defined as [21].

$$x_{k+1} = F(x_k, u_k) \tag{11}$$

$$u_k = u(x_k) \tag{12}$$

The sliding manifold is attained at each sampling point i.e., $s(k_{k+1}),\quad \forall k = 0,1,\ldots$ is fulfilled.

This is true because $F(x(0), u)$ tends to $x(0)$ as $\Delta t \to 0$, the function $u(x(0), \Delta t)$ may exceed the available control resources u_0 Using the discrete time sliding mode, the sliding manifold is defined as

$$s(x_k) = x_k - x_{ref,k} \tag{13}$$

Evaluating the sliding manifold at $(k+1)$, we obtain

$$s_{k+1} = F(x_k, u_k) - x_{ref,k+1} \tag{14}$$

Then, the equivalent control $u_{eq}(x_k, k)$ is calculated as [20]

$$u_{eq}(x_k, k) = -\left[F(x_k, k) - x_{ref,k+1}\right] \tag{15}$$

It is appropriate to add a stabilizing term $u_n(x_k, k)$, to reach the sliding manifold asymptotically [21]

$$u_n(x_k, k) = -(ks_k) \tag{16}$$

where k is Schur matrix.

Considering the boundedness of the control signal $\| u_c(x_k, k) \| < u_0\ ,\ u_0 > 0$, the following control law is selected [20]

$$u(x_k, k) = \begin{cases} u_c(x_k, k) & if\ \ ||u_c(x_k, k)|| < u_0 \\ u_0 \dfrac{u_{eq}(x_k, k)}{\left||u_{eq}(x_k, k)|\right|} & if\ \ ||u_c(x_k, k)|| \geq u_0 \end{cases} \tag{17}$$

Where $||.||$stands for the Euclidean norm and $u_c(x_k, k) = u_{eq}(x_k, k) + u_n(x_k, k)$.

IV. Buck-Boost Neural Control Analysis

A. System Modeling

The used DC-DC converter in this application is composed of a boost and buck converters. The first one is used under charge conditions while the second one is used under discharge conditions. The boost converter model is defined as [22].

$$x_{1,k} = \left(1 - \frac{ts}{RC}\right) x_{1,k} - \frac{ts}{c} x_{2,k} \tag{18}$$

$$x_{2,k} = x_{2,k} + \frac{ts}{L} U_{btt} u_c \tag{19}$$

The buck converter model is given by [22]

$$x_{1,k} = \left(1 - \frac{ts}{RC}\right) x_{1,k} + \frac{ts}{c} x_{2,k} \tag{20}$$

$$x_{2,k} = x_{2,k} + \frac{ts}{L} U_{btt} u_c \tag{21}$$

ISSN-2523-6830

where $x_{1,k}$ is the Buck-Boost converter output voltage, $x_{2,k}$ is the Buck-Boost converter output current both with the inductance L(H), resistance load R (Ω), capacitor (F) C, and t_s sampling time.

B. Neural Controller Design

To control the current flow and ensure the charging and discharging operation modes, an RHONN has been used to approximate the buck-boost converter behaviors and then the sliding mode controller is synthesized. Knowing the adaptive nature of the RHONN, and the similitude between the buck and boost converter models a single identifier is proposed for both cases as

$$\widehat{x_{1,k}} = \omega_{1,1}(k)S(x_1) + \omega_{1,2}(k)S(x_2) + w_{1,3}S(x_1)S(x_2) + \varpi_1 x_2 \quad (22)$$

$$\widehat{x_{2,k}} = \omega_{2,1}(k)S(x_2) + \omega_{2,2}(k)S(x_1) + w_{2,3}S(x_1)S(x_2) \quad (23)$$

Equations (22) and (23) can be rewritten as follows

$$\widehat{x_k} = \hat{F}(x_k) + \hat{B}u(x_k, k) \quad (24)$$

$$\widehat{y_k} = x_{2,k}k \quad (25)$$

where $\left[\widehat{x_{1,k}}, \widehat{x_{2,k}}\right]^T$ are the estimated dynamics of $\left[x_{1,k}, x_{2,k}\right]^T$, u_k is the input signal, $\widehat{y_k}$ is the output to be tracked, and $\hat{B}$ is the control matrix defined as $\hat{B} = diag[0, \varpi_2]$. Since the proposed neural model is formulated in the triangular form, the control of the last dynamics is only needed [20]. So, by using the same steps as in (11)-(17) the sliding surface at $k+1$ is obtained as

$$s_{k+1} = \omega_{2,1}(k)S(x_2) + \omega_{2,2}(k)S(x_1) + w_{2,3}S(x_1)S(x_2)\varpi_2 u(x_k, k) - x_{ref,k+1} \quad (26)$$

Then, the equivalent control is calculated as follows

$$u_{eq}(x_k, k) = -\frac{1}{\varpi_2}\left[\omega_{2,1}(k)S(x_2) + \omega_{2,2}(k)S(x_1) + w_{2,3}S(x_1)S(x_2) - x_{ref,k+1}\right] \quad (27)$$

And the NSMC is implemented as follows.

$$u(x_k, k) = \begin{cases} u_c(x_k, k) & if \ ||u_c(x_k, k)|| < u_0 \\ u_0 \frac{u_{eq}(x_k, k)}{||u_{eq}(x_k, k)||} & if \ ||u_c(x_k, k)|| \geq u_0 \end{cases} \quad (28)$$

With $u_c(x_k, k) = u_{eq}(x_k, k) + u_n(x_k, k)$, $u_n(x_k, k) = -(ks_k)$, where k is Schur matrix, and u_0 is the control upper bound.

V. Simulation results

The proposed control scheme as well the respective MES and AES are implemented and evaluated using the SimPower System toolbox of MATLAB. The parameters of the AES and MES are listed in Tab. 1

Description	Unit
Converter Resistance R.	50 Ω
Converter Inductance L	1.5 $e^{-3}H$
Converter Capacitance C	100 e^{-3} F
Super-capacitor voltage V_{sc}	350 V
Battery Bank Voltage V_c	450 V
Initial SOC	80%
Sampling time (t_s)	$1e^{-5}s$

Table 1 Parameters of the AES and MES

A. Neural Identification

The implemented RHONN identification allows to achieve adequate estimation of system states, which are in this case, the voltage x_1, k and current x_2, k during different operation modes. Fig.5 illustrates the neural identification of the voltage $(x_1, k)$and their respective neural weights evolution.

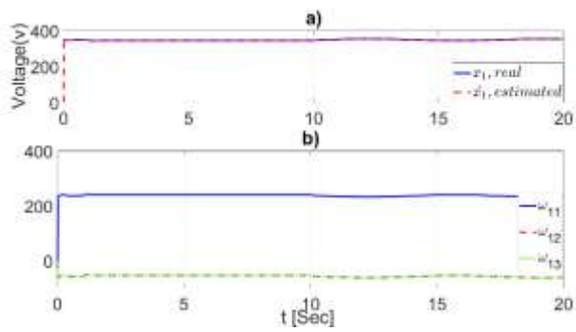

Figure 5 a) Voltage identification (x_1, k) b) NN_s weights

Fig. 6 presents the neural identification of the current (x_2, k) and their respective neural weights dynamics.

From the obtained results, it is clear to observe that the proposed RHONN identifiers successfully approximate the voltage and current dynamics of the AES even a varying-time trajectories are applied. In addition, all neural weights are bounded.

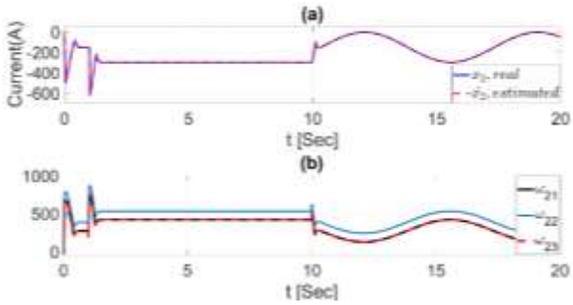

Figure 6. a) Current identification (x_2, k) b) NN_s weights

B. Trajectory Tracking

In this test, the objective is to demonstrate the trajectories tracking of the AES voltage and current. To do such, a varying-time voltage reference x_1, r is used where it is initiated in $350\ V$ and then decrease to $345\ V$ after $10\ s$ and then, this reference is changed to a sinusoidal function. Fig 7 presents the obtained results for the voltage (x_1, k) at the output of the Buck-boost converter used in the AES system, which is controller using NSMC.

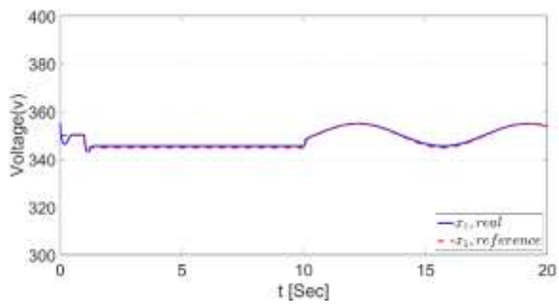

Figure 7 Voltage Trajectory Tracking

Fig 8 demonstrates the behavior of the current (x_2, k) as measured at inductor of the Buck-boost converter.

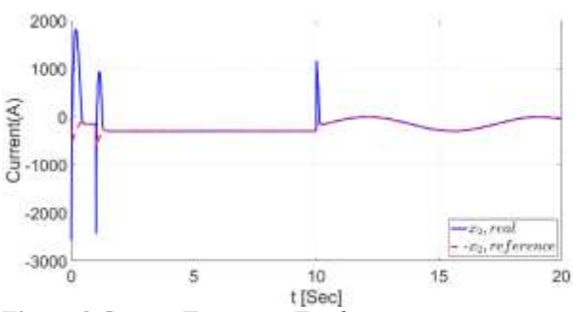

Figure 8 Current Trajectory Tracking

Fig. 9 displays the charging and discharging modes of the AES. In the charging operating mode, $t = 0\ s$ to $t = 10\ s$, the boost mode is selected while the buck mode is used during the discharging mode $t = 10\ s$ to $t = 20\ s$.

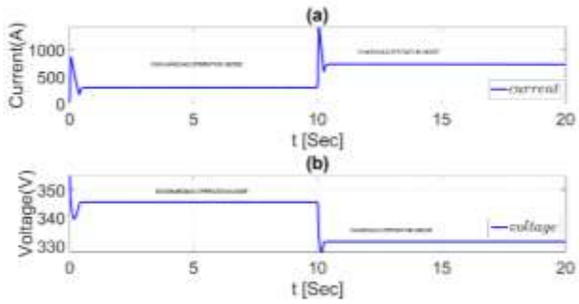

Figure 9 AES charging and discharging

From the obtained results, we can see that the proposed control scheme (NSMC) ensures adequate trajectories tracking of the AES voltage and current even a time-varying references are applied. In addition, the proposed controller assures the charge and discharge operation modes of the AES.

Fig. 10 illustrates a comparison between the MES discharging behavior with and without AES. Form the obtained results, the MES performance is improved by using the AES since the MES discharging behavior without AES is fast than when this last is activated.

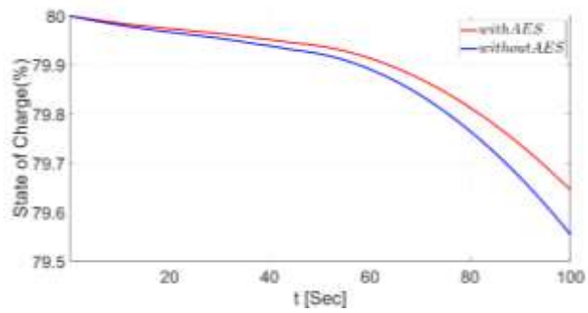

Figure 10 Comparison of variables with and without the regenerative braking

VI. Conclusion

This paper presents NSMC of a regenerative braking system used in the EVs. The proposed control scheme is used to control the AES composed of a buck-boost converter and super-capacitor with the objective to recover the energy during breaking and participating in power supply of the MES.

The RHONN identifier trained by an EKF is build-up to approximate the AES behavior under different operation modes; then, the Sliding mode controller is synthesized. The proposed control scheme is tested for trajectory tracking of time-varying references and in the presence of AES different operation modes. The obtained results illustrate the effectiveness of the proposed control scheme where the trajectories tracking of AES voltage and current are achieved and the charging and discharging mode is ensured. In addition, the MES behavior is enhanced by using the AES, which helps to improve the discharging time of the MES and extend the operation time of the EV.

As a future work, the proposed control scheme and other ones will be implemented in real-time and tested in the presence of parameter variation and disturbances.

Finally, the used controller in this paper presents a simple control algorithm, which can be used in the industrial EV applications.

Acknowledgments

This work has been funded by Consejo Nacional de Ciencia y Tecnología (CONACYT) [1085717] and Universidad Autónoma del Carmen (UNACAR) [120664].

References

[1] Pavlović, T., Mirjanić, D., Mitić, I. R., & Stanković, A. M. (2019, June). The Impact of Electric Cars Use on the Environment. In *International Conference "New Technologies, Development and Applications"* (pp. 541-548). Springer, Cham. https://doi.org/10.1007/978-3-030-18072-0_62

[2] Yoong, M. K., Gan, Y. H., Gan, G. D., Leong, C. K., Phuan, Z. Y., Cheah, B. K., & Chew, K. W. (2010, November). Studies of regenerative braking in electric vehicle. In *2010 IEEE Conference on Sustainable Utilization and Development in Engineering and Technology* (pp. 40-45). IEEE. https://doi.org/10.1109/STUDENT.2010.5686984

[3] Tie, S. F., & Tan, C. W. (2013). A review of energy sources and energy management system in electric vehicles. *Renewable and sustainable energy reviews*, *20*, 82-102. https://doi.org/10.1016/j.rser.2012.11.077

[4] García-Villalobos, J., Zamora, I., San Martín, J. I., Asensio, F. J., & Aperribay, V. (2014). Plug-in electric vehicles in electric distribution networks: A review of smart charging approaches. *Renewable and Sustainable Energy Reviews*, *38*, 717-731. https://doi.org/10.1016/j.rser.2014.07.040

[5] Hannan, M. A., Azidin, F. A., & Mohamed, A. (2014). Hybrid electric vehicles and their challenges: A review. *Renewable and Sustainable Energy Reviews*, *29*, 135-150. https://doi.org/10.1016/j.rser.2013.08.097

[6] Ortúzar, M., Moreno, J., & Dixon, J. (2007). Ultracapacitor-based auxiliary energy system for an electric vehicle: Implementation and evaluation. *IEEE Transactions on industrial electronics*, *54*(4), 2147-2156. https://doi.org/10.1109/TIE.2007.894713

[7] Zhang, L., & Cai, X. (2018). Control strategy of regenerative braking system in electric vehicles. *Energy Procedia*, *152*, 496-501. https://doi.org/10.1016/j.egypro.2018.09.200

[8] Indragandhi, V., Selvamathi, R., Gunapriya, D., Balagurunathan, B., Suresh, G., & Chitra, A. (2021, November). An Efficient Regenerative Braking System Based on Battery-Ultracapacitor for Electric Vehicles. In *2021 Innovations in Power and Advanced Computing Technologies (i-PACT)* (pp. 1-5). IEEE. https://doi.org/10.1109/i-PACT52855.2021.9696557

[9] Quintero-Manriquez, E., Sanchez, E. N., Antonio-Toledo, M. E., & Munoz, F. (2021). Neural control of an induction motor with regenerative braking as electric vehicle architecture. *Engineering Applications of Artificial Intelligence*, *104*, 104275. https://doi.org/10.1016/j.engappai.2021.104275

[10] J. Guo, J. Xiaoping, and L. Guangyu, "Performance evaluation of an anti-lock braking system for electric vehicles with a fuzzy sliding mode controller," Energies, vol. 7, pp. 6459–6476, Aug. 2014. https://doi.org/10.3390/en7106459

[11] Rajendran, S., Spurgeon, S., Tsampardoukas, G., & Hampson, R. (2018). Intelligent sliding mode scheme for regenerative braking control. *IFAC-PapersOnLine*, *51*(25), 334-339. https://doi.org/10.1016/j.ifacol.2018.11.129

[12] Li, X., Xu, L., Hua, J., Li, J., & Ouyang, M. (2008, October). Regenerative braking control strategy for fuel cell hybrid vehicles using fuzzy logic. In *2008 International Conference on Electrical Machines and Systems* (pp. 2712-2716). IEEE.

[13] Sanchez, E. N., Alanís, A. Y., & Loukianov, A. G. (2008). *Discrete-time high order neural control*. Warsaw: Springer. https://doi.org/10.1007/978-3-540-78289-6

[14] Lopez-Franco, M., Sanchez, E. N., Alanis, A. Y., Lopez-Franco, C., & Arana-Daniel, N. (2015). Decentralized control for stabilization of nonlinear multi-agent systems using neural inverse optimal control. *Neurocomputing*, *168*, 81-91. https://doi.org/10.1016/j.neucom.2015.06.012

[15] Djilali, L., Vega, C. J., Sanchez, E. N., & Ruz-Hernandez, J. A. (2021). Distributed Cooperative Neural Inverse Optimal Control of Microgrids for Island and Grid-Connected Operations. *IEEE Transactions on Smart Grid*, *13*(2), 928-940. https://doi.org/10.1109/TSG.2021.3132640

[16] Rios, Y. Y., Garcia-Rodriguez, J. A., Sanchez, E. N., Alanis, A. Y., & Ruiz-Velázquez, E. (2018, November). Rapid Prototyping of Neuro-Fuzzy Inverse Optimal Control as Applied to T1DM Patients. In *2018 IEEE Latin American Conference on Computational Intelligence (LA-CCI)* (pp. 1-5). IEEE. https://doi.org/10.1109/LA-CCI.2018.8625241

[17] Cao, J., Cao, B., Xu, P., & Bai, Z. (2008, July). Regenerative-braking sliding mode control of electric vehicle based on neural network identification. In *2008 IEEE/ASME International Conference on Advanced Intelligent Mechatronics* (pp. 1219-1224). IEEE. https://doi.org/10.1109/AIM.2008.4601836

[18] Alanis, A. Y., Sanchez, E. N., & Loukianov, A. G. (2007). Discrete-time adaptive backstepping nonlinear control via high-order neural networks. *IEEE Transactions on Neural Networks*, *18*(4), 1185-1195. https://doi.org/10.1109/TNN.2007.899170

[19] Rovithakis, G. A., & Christodoulou, M. A. (2012). *Adaptive control with recurrent high-order neural networks: theory and industrial applications*. Springer Science & Business Media. https://doi.org/10.1007/978-1-4471-0785-9

[20] Utkin, V., Guldner, J., & Shi, J. (2017). *Sliding mode control in electro-mechanical systems*. CRC press. https://doi.org/10.1201/9781420065619

[21] Sánchez, E. N., & Djilali, L. (2020). *Neural Control of Renewable Electrical Power Systems* (Vol. 278). Springer Nature. https://doi.org/10.1007/978-3-030-47443-0

[22] Djilali, L., Sanchez, E. N., Ornelas-Tellez, F., Avalos, A., & Belkheiri, M. (2019). Improving microgrid low-voltage ride-through capacity using neural control. *IEEE Systems Journal*, *14*(2), 2825-2836. https://doi.org/10.1109/JSYST.2019.2947840

ISSN-2523-6830

Article **Journal Innovative Design**
December, 2022 Vol.6 No.15 19-25

MAC-based Artificial Neural network for voice command recognition

Red Neuronal Artificial basada en MAC para reconocimiento de comandos de voz

RODRÍGUEZ-PONCE, Rafael†*

Universidad Politécnica de Guanajuato, Ingeniería en Robótica

ID 1st Author: *Rafael, Rodríguez-Ponce* / **ORC ID:** 0000-0001-5006-5580, **CVU CONACYT ID**: 209261

DOI: 10.35429/JID.2022.15.6.19.25 Received July 23, 2022; Accepted October 30, 2022

Abstract

Artificial neural networks are one of the most popular families of machine learning algorithms of this decade. Although they exist since the middle of the last century, until recent years with the improvement of technology, they are being widely used in fields such as character, image, and voice recognition. There is a large number of works implementing neural networks for speech recognition; however, the approach has usually been for operation on a personal computer, which is not suitable for mobile applications. This article presents a neural network for voice command recognition, implemented in a compact FPGA card with low computational resources. In addition, it uses a multiplication and accumulation unit, called MAC, with which it achieves a smaller size and higher speed. This paper will be of interest to students or researchers working on machine learning mobile applications.

Automatic speech recognition, Mel-frequency cepstral coefficients (MFCC), Field programmable gate array (FPGA)

Resumen

Las redes neuronales artificiales son en una de las familias de algoritmos de machine learning más populares de esta década. Aunque existen desde mediados del siglo pasado, hasta recientes años con la mejora de la tecnología, están siendo ampliamente utilizados en campos tales como reconocimiento de caracteres, imágenes y voz. Existe un gran número de trabajos de implementación de redes neuronales para reconocimiento de voz, sin embargo el enfoque normalmente ha sido para funcionamiento en una computadora personal, lo cual no es adecuado para aplicaciones móviles. En este artículo se presenta una red neuronal para reconocimiento de comandos de voz, implementada en una tarjeta FPGA compacta y de bajos recursos computacionales. Además, utiliza una unidad de multiplicación y acumulación, denominada MAC, con la cual logra un menor tamaño y mayor velocidad. Este documento será de interés a estudiantes o investigadores interesados en aplicaciones móviles de machine learning.

Reconocimiento automático de voz, Coeficientes cepstrales de frecuencias de Mel, Matriz reconfigurable de compuertas digitales

Citation: RODRÍGUEZ-PONCE, Rafael. MAC-based Artificial Neural network for voice command recognition. Journal Innovative Design. 2022, 6-15: 18-25

*Correspondence to the Author (e-mail: rrodriguez@upgto.edu.mx)
† Researcher contributing as first author.

Introduction

Nowadays, we live in a time when digital electronics are an integral part of our lives. They are found in computers and communication equipment, household devices, entertainment equipment, and power tools, among others; however, in some instances it would be desirable for the device or equipment to be able to carry out, in some way, a learning process without the need for user intervention, in other words, to contain some type of artificial intelligence.

An artificial neuron is a mathematical-computational model with various inputs and outputs, which tries to emulate the functioning and learning of a biological neuron (Hudson and Cohen, 2012). Thanks to the latest advances in computing technology, they have begun to be used mainly in digital applications such as character recognition (Liu, *et al*., 2020), image classification (Dong, *et al*., 2022), text generation (Zhang, *et al*., 2019), language translation (Nguyen, *et al*., 2019) autonomous driving (Chen, *et al.*, 2021), and many others; however, an application that has attracted great interest in recent years is voice-command recognition (Nassif, *et al.*, 2019).

For the implementation of a neural network, it is common to use a personal computer; however, for mobile applications, a more compact, lightweight electronic system with low power consumption is necessary. For these cases, a microcontroller or an FPGA is the most recommended option, although they are more limited in computational resources, compared to a computer. (Ma, Cao and Sao, 2018).

The main operation of a neural network can be summarized as a weighted sum of all the values of the network inputs. Thus, its implementation requires a large number of addition and multiplication operations. If the network is very large all the arithmetic resources of the system can be exhausted in a small device. However, using a more robust device implies a greater consumption of time and power. (Zu y Sutton, 2003).

Although multiple implementations of neural networks have already been made for voice command recognition, a personal computer with robust graphics processing units (GPU) and using high-level programming languages are normally used. Even though they have provided excellent results, they are not suitable for being incorporated into mobile technology (Lyashenko, *et al*., 2021) due to all the computational resources and electrical power they require.

In this work, it was decided to implement an artificial neural network for voice-command recognition on an FPGA since, despite having low computational resources; it allows the design of user-customized digital architectures. In this project, the system is based on the use of a single Multiply and Accumulate (MAC) unit for each neuron, allowing a low number of arithmetic elements used.

A MAC unit is a digital architecture that allows the weighted sum required by the neural network, to be executed cyclically. So no matter how many inputs the neuron has, it always uses a single MAC unit (Nedja, *et al.*, 2009). Furthermore, the FPGA already has these high-speed MAC units embedded in its digital architecture, so there is no need to use logic gates for its implementation.

There are different methods for extracting relevant information from the voice signal (Cabral, Fikai and Tamura, 2019); however, one that has shown very good results is the Mel Frequency Cepstral Coefficients (MFCC). These coefficients are obtained through a filter bank whose operation is similar to that of the human ear (Jo, Yoo and Park, 2015).

In this paper, a network of six single-layer neurons was implemented in an FPGA, for the identification of six voice commands. First, the voice signals are processed using MFCC to extract the most relevant information. Then, these coefficients are fed to a network of six neurons with eight inputs each. The network was trained with 4,000 voice commands from men and women, adults and children, achieving a general accuracy greater than 95%.

ISSN-2523-6830

This work can be very interesting and useful for students, teachers, or researchers interested in the implementation of neural networks for voice command identification in mobile devices.

Artificial Neuron

An artificial neuron also called a perceptron, is a computational function, which has several data inputs and a single output. The neuron uses this input data to perform a weighted sum of them. This weighting is given by a weight that is assigned to each of the input connections, and in this way, changes the intensity with which each input affects the behavior of the neuron. It is also assigned a bias value, which is represented as an internal connection of the neuron. After the sum of the input/weight products and the bias, an activation function such as a sigmoid is applied, which is a non-linear function and, in a certain way, distorts the output value so that gradually, large values converge to 1 and small values converge to 0. The structure of an artificial neuron is shown in Figure 1.

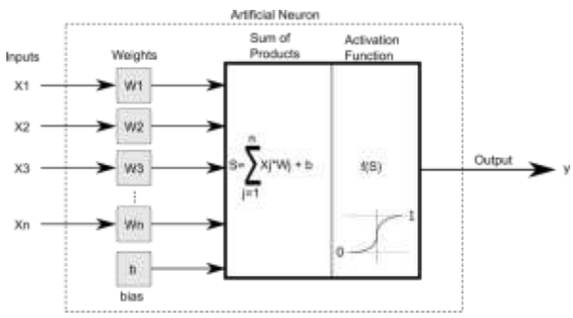

Figure 1 Structure of an artificial neuron
Source: Self-Made.

The importance of the activation function occurs mainly when several neurons are chained together to form a neural network that achieves a deeper level of learning. Thus, the non-linearity of each neuron allows a more complex function. Otherwise, it would behave such as a simple linear regression function (Pomerat, Segev and Datta, 2019).

Mel Frequency Cepstral Coefficients

A widely used technique for speech recognition is Mel Frequency Cepstral Coefficients or MFCC. This method is used to extract the most relevant information from the audio signal and feed it to the artificial neuron.

For the application of this technique to voice commands, Librosa was used, which is a computational package in the Python programming language designed for the analysis of music and audio signals. (McFee, *et al.*, 2015).

The information extraction procedure is described below and shown in Figure 2. First, the Discrete Fourier Transform (DFT) is applied to obtain the spectral content of the audio signal, passing from the time domain to the frequency domain. It is then passed through a filter bank on the Mel scale, which extracts the most relevant information in certain frequency ranges, which is similar to the functioning of the human ear. This scale is linear below 1 kHz and logarithmic above this threshold (Jo, Yoo and Park, 2015). Finally, the logarithm of these energies and the discrete cosine transform (DCT) are obtained to again obtain information in the time domain, similar to the inverse Fourier transform, except that the coefficients obtained with the DCT they are always real numerical values.

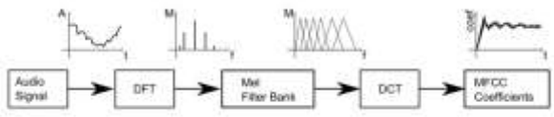

Figure 2 Block diagram for the MFCC technique
Source: Self-Made.

MAC Unit Architecture

A MAC unit is a digital structure that is used to perform a sum of products of any length, using a single addition and multiplication operation cyclically. The benefit of using these structures is that it allows savings in arithmetic resources in an FPGA. (Mohindroo, Paliwal and Suneja, 2020).

The digital structure of a MAC unit is shown in Figure 3 and described as follows. Firstly, there is the input of two data values which are multiplied arithmetically. The result of the product is now added to the contents of an accumulator, which is zero in the very first cycle, and this result in turn is stored in the accumulator.

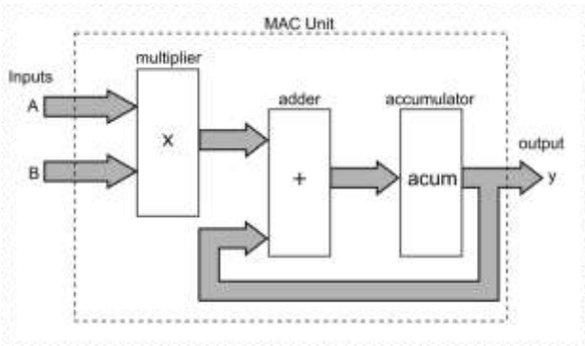

Figure 3 MAC unit structure
Source: Self-Made.

In the next cycle, the next two data inputs are multiplied and added to the current contents of the accumulator, which are then stored in the accumulator for the next cycle. This process is repeated indefinitely, depending on the number of data values to be multiplied. Once the multiplication and addition process is completed, the final result can be obtained at the output of the MAC unit. It is worth mentioning that, for the control of input data and process repetitions, a Finite State Machine (FSM) is used, which is a sequential digital structure commonly applied for process control in digital systems.

In Figure 4(a) the complete diagram of the MAC unit is shown, and Figure 4(b) shows the control logic that follows the FSM of this unit, which is described as follows. To start the multiplication and accumulation process, the required number of N cycles is indicated to the FSM and a start signal is given. Each input data is multiplied and added with the content of the accumulator register, and the FSM sends a signal so that this result is stored in the register again. A digital counter keeps track of the required cycles and, at the same time, outputs this data, which will be used to synchronize the input of the MFCC coefficients to the neuron. Once the process is finished, the FSM sends a signal to an output register so that it allows the final result to be output, and a completion signal is also sent to the next block, to indicate that the result can be retrieved.

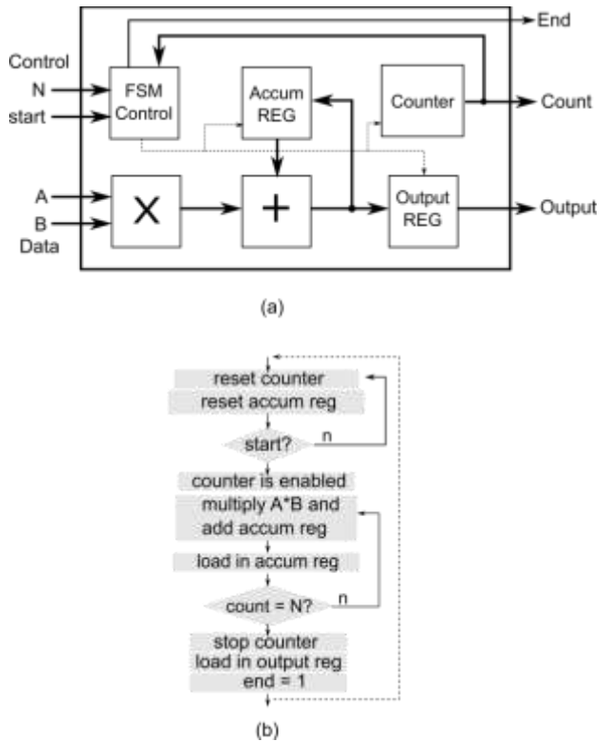

Figure 4 (a) Complete structure of the MAC unit and (b) the corresponding FSM logic control
Source: Self-Made.

The main advantage of the MAC structure is that a sum of products of any size can be achieved with a single multiplier and adder. Despite being cyclical, it can be carried out at a very high speed when implemented in an FPGA. (Mohindroo, Paliwal and Suneja, 2020).

System architecture

The description of the complete neural network functionality has been divided into two parts for ease of understanding. Firstly, the digital architecture required for data input to the neuron is shown when the neuron training is disabled, and later, when training is enabled.

Neural network architecture with training disabled

When the neuron training is disabled, only the products of the coefficients and the weights are carried out, the sigmoid activation function is applied and the result is sent to the output (Figure 5). This process is controlled by an FSM which is in charge of synchronizing the input of weights and coefficients to the MAC unit so that, one by one, they are multiplied and accumulated.

The initial weights used are random values stored in a Look-Up Table (LUT), which are only updated when the neuron training is enabled. Once the sum of products operation is finished, the bias value is added, which initially is also a random value and is updated in training mode.

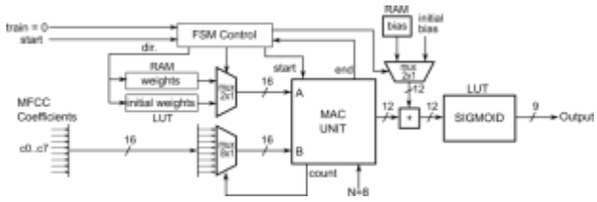

Figure 5 Digital structure for the artificial neuron with training disabled
Source: Self-Made

Finally, the data is passed to a LUT for the sigmoid function, which has 12 input bits and 9 output bits.

Neural network architecture with training enabled

When the neuron training is enabled, in addition to the weighted sum and the application of the sigmoid function, the error between the current output data and the desired output is calculated. This error value is used to carry out the correction of the weights and the bias so that the error tends to be close to zero.

First, an adjustment factor is calculated using gradient descent. This correction value is added to the weights and bias and stored back in memory to be used in the next training cycle. Again, the FSM is responsible for controlling the entire process of error calculation, gradient descent, and weight/bias correction. (Figure 6).

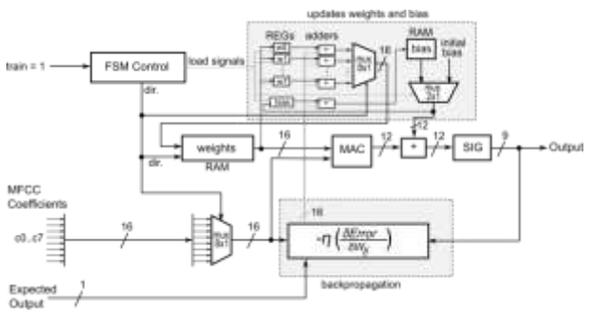

Figure 6 Digital structure for the artificial neuron with training and learning mode enabled
Source: Self-Made

It is worth mentioning that the input and output width of the neuron is completely generic, so they can be easily changed by simply adjusting the parameter at the time of structure generation, without the need for code modification.

Complete Neural Network

The architecture shown above in Figure 6 represents the neuron for a single voice command. In the case of this paper, six voice commands were selected, for which the network is made up of six identical neurons (Figure 7), which are executed and trained simultaneously. At the output of the network, there is a magnitude comparator, which outputs a logical 1 for the signal with the highest magnitude, and a logical 0 for all others.

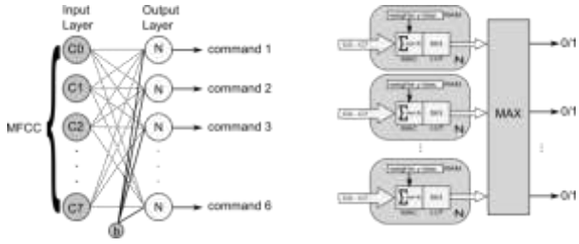

Figure 7 Digital structure for the complete neural network
Source: Self-Made

Testing and Results

In the first instance, 4000 voice signals of six different commands in Spanish were collected, these being: stop, forward, up, down, left, and right. The intention of using these six commands is for a future project of voice control for an unmanned aircraft or drone.

Voice commands were collected from men and women of different ages, in a closed environment without noise. All voice commands were set to a 1-second duration, being digitally recorded on a cell phone or personal computer. The information preparation process is shown in Figure 8 and described below.

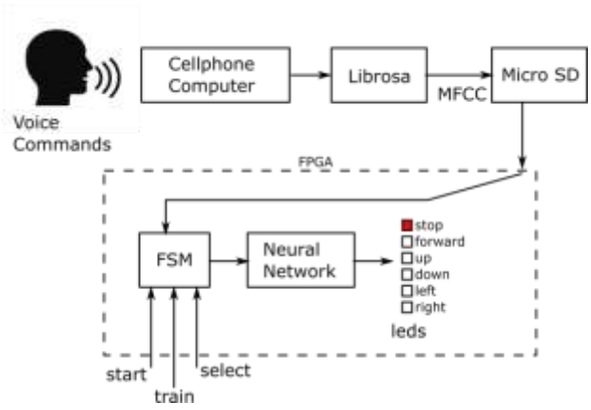

Figure 8 Voice command preparation and processing process
Source: Self-Made

First, the voice signals were processed in Python using the Librosa libraries for the extraction of the MFCC coefficients and stored in a microSD digital memory card. It is worth mentioning that, in this application, it is possible to select the number of MFCC coefficients to extract. However, the greater the number of coefficients, the greater the number of inputs required in the neuron and, therefore, the greater the number of operations to be carried out in the FPGA. After several tests, it was found that eight MFCC coefficients were more than enough to properly distinguish each of the voice commands.

Subsequently, the microSD memory is inserted into the FPGA containing the artificial neuron (Figure 7), and the training process of the neural network is started using 2000 of the voice commands stored in memory. These commands are fed one by one and are processed at high speed so that 5 seconds were enough to train the entire network.

For the network validation, the remaining 2000 voice commands were used, which are fed to the neuron every second, to be verified in the FPGA card's LEDs. The success rate for voice commands is shown in Table 1.

Commands	Voiced	Successful	Percentage
Stop	330	318	96.3%
Forward	330	315	95.4%
Up	330	321	97.2%
Down	330	325	98.4%
Left	350	334	95.4%
Right	330	323	97.8%

Table 1 Success rate for each voice command
Source: Self-Made

The FPGA board used is an Intel-Altera DE1-SoC, with a Cyclone V and a 150 MHz clock frequency.

Conclusion

In this work, a neural network for the identification of six voice commands was presented. This network was implemented in an FPGA using a single MAC unit for each neuron. With this architecture, the identification of the commands coming from adults and children of both sexes was achieved, with a success greater than 95%.

This work will be of great interest to students, teachers, or researchers in search of a simple and efficient alternative for the implementation of neural networks.

References

Cabral F.S., Fukai H. and Tamura S. (2019). Feature Extraction Methods Proposed for Speech Recognition Are Effective on Road Condition Monitoring Using Smartphone Inertial Sensors, *Sensors, 19*(1), 1-20. DOI: 10.3390/s19163481.

Chen L., Lin S., Lu X., Cao D., Wu H., Guo C., Liu C. and Wang F.Y. (2021). Deep Neural Network Based Vehicle and Pedestrian Detection for Autonomous Driving: A Survey, *IEEE Trans. Int. Transp. Sys., 22*(6), 3234-3246. DOI: 10.1109/TITS.2020.2993926.

Dong Y., Liu Q., Du B. and Zhang L. (2022). Weighted Feature Fusion of Convolutional Neural Network and Graph Attention Network for Hyperspectral Image Classification, *IEEE Trans. Image Proc., 31*(1), 1559-1572. DOI: 10.1109/TIP.2022.3144017.

Hudson D. and Cohen M. (2012). *Neural Networks and Artificial Intelligence for Biomedical Engineering*. Wiley-IEEE Press, ISBN: 978-0-470-54535-5. DOI: 10.1109/9780470545355.

Jo J., Yoo H. and Park I.C. (2015). Energy-Efficient Floating-Point MFCC Extraction Architecture for Speech Recognition Systems, *IEEE Trans. VLSI Syst., 24*(2), 754-758. DOI: 10.1109/TVLSI.2015.2413454.

Liu X., Hu B., Chen Q., Wu X. and You J. (2020). Stroke Sequence-Dependent Deep Convolutional Neural Network for Online Handwritten Chinese Character Recognition, *IEEE Trans. Neural Netw. Learn Syst., 31*(11), 4637-4648. DOI: 10.1109/TNNLS.2019.2956965.

Lyashenko V., Laariedh F., Sotnik S. and Ahmad M.A. (2021). Recognition of voice commands based on Neural Network, *TEM Journal*, *10*(2), 583-591, DOI: 10.18421/TEM102-13.

Ma Y., Cao Y. and Sao J.S. (2018). Optimizing the Convolution Operation to Accelerate Deep Neural Networks on FPGA, *IEEE Trans. VLSI Syst.*, *26*(7), 1354-1367. DOI: 10.1109/TVLSI.2018.2815603.

McFee B., Raffel C., Liang D., Ellis DPW., McVicar M., Battenberg E. and Nieto O. (2015). *Librosa: audio and music analysis in python*, In Proceedings of the 14th python in science conference, 18-25. DOI: 10.5281/zenodo.6097378.

Mohindroo B., Paliwal A. and Suneja K. (2020). *FPGA-based Faster Implementation of MAC Unit in Residual Number System, INCET* International Conference on Emerging Technology, Balgaum, India. DOI: 10.1109/INCET49848.2020.9154105

Nassif A.B., Shahin I., Attili I., Azzeh M. and Shaalan K. (2019). Speech Recognition Using Deep Neural Networks: A Systematic Review, *IEEE Access*, *7*(1), 19143-19165. DOI: 10.1109/ACCESS.2019.2896880.

Nedja N., Da Silva R.M., Mourelle L.M. and Da Silva M.V.C. (2009). Dynamic MAC-based architecture of artificial neural networks suitable for hardware implementation on FPGAs, *Neurocomputing*, *72*(1), 2171-2179. DOI: 10.1016/j.neucom.2008.06.027.

Nguyen Q.P., Vo A.D., Shin J.C., Tran P. and Ock C.Y. (2019). Korean-Vietnamese Neural Machine Translation System with Korean Morphological Analysis and Word Sense Disambiguation, *IEEE Access*, *7*(1), 32602 – 32616. DOI: 10.1109/ACCESS.2019.2902270.

Pomerat J., Segev A. and Datta R. (2019). On Neural Network Activation Functions and Optimizers in Relation to Polynomial Regression, *IEEE Int. Conference on Big Data*, Los Angeles, Calif. USA. DOI: 10.1109/BigData47090.2019.9005674.

Zhang R., Wang Z., Yin K. and Huang Z. (2019). Emotional Text Generation Based on Cross-Domain Sentiment Transfer, *IEEE Access*, *7*(1), 100081 - 100089. DOI: 10.1109/ACCESS.2019.2931036.

Zu J. and Sutton P. (2003). *FPGA Implementations of Neural Networks - A Survey of a Decade of Progress*, Ed. Springer-Verlag, Berlin, 1062-1066. DOI: 10.1007/978-3-540-45234-8_120.

Article **Journal Innovative Design**
December, 2022 Vol.6 No.15 26-34

Spur gears with contact ratio less than unity

Engranes rectos con relación de contacto menor a la unidad

JIMÉNEZ-RABIELA, Homero†*, VÁZQUEZ-GONZÁLEZ, Benjamín, RAMÍREZ-CRUZ, José Luis and BRAVO-ACOSTA, Adrian Gustavo

Universidad Autónoma Metropolitana, Unidad Azcapotzalco, División de Ciencias Básicas e Ingeniería, Departamento de Energía

ID 1st Author: *Homero, Jiménez-Rabiela* / **ORC ID**: 0000-0002-1549-0853, **Researcher ID Thomson**: S-2299-2018, **CVU CONACYT ID**: 123386

ID 1st Co-author: *Benjamín, Vázquez-González* / **ORC ID**: 0000-0002-9030-5662, **Researcher ID Thomson**: S-2417-2018, **CVU CONACYT ID**: 25749

ID 2nd Co-author: *José Luis, Ramírez-Cruz* / **ORC ID**: 0000-0003-0762-2630, **Researcher ID Thomson**: G-3405-2019, **CVU CONACYT ID**: 921268

ID 3rd Co-author: *Adrian Gustavo, Bravo-Acosta* / **ORC ID**: 0000-0001-57975317, **Researcher ID Thomson**: 2272-2018, **CVU CONACYT ID**: 334391

DOI: 10.35429/JID.2022.15.6.26.34 Received July 23, 2022; Accepted October 30, 2022

Abstract

The objective of this research is to evaluate the design of a pair of spur gears and another analogous pair with a contact ratio of less than unity. Considering two pairs of normalized gears with equal diametral pitches and pressure angles, as well as equal pitch radii in their driving gears and equal pitch radii in their driven gears. For the first pair of gears with normalized tooth numbers, the contact ratio greater than unity es obtained. For the second pair of gears, the number of teeth is proportionally reduced, consequently obtaining a contact ratio of less than one. For both pairs, the maximum von Mises stresses are obtained using the finite element method. The pairs are compared qualitatively and quantitatively. This work contributes with novel elements of judgment for a better decision making of the industrialists interested in reducing the problems of normalized spur gears such as noise, abrasive wear, adhesive wear, temperature, and efforts induced by the overlapping relationship between coupled teeth; proposing them a practical solution that will open new avenues of research.

Noise, Temperature, Abrasion

Resumen

El objetivo de esta investigación es evaluar el diseño de un par de engranes rectos y además otro par análogo con relación de contacto menor a la unidad. Considerando dos pares de engranes normalizados con pasos diametrales y ángulos de presión iguales además con radios de paso iguales en sus engranes motrices y con radios de paso iguales en sus engranes movidos. Para el primer par de engranes con números de dientes normalizados se obtiene la relación de contacto mayor a la unidad. Para el segundo par de engranes se reducen proporcionalmente los números de dientes obteniéndose consecuentemente una relación de contacto menor a la unidad. Para ambos pares se obtienen los esfuerzos máximos de Von Mises usando el método de los elementos finitos. Los pares se comparan cualitativa y cuantitativamente. Este trabajo contribuye con elementos de juicio novedosos para una mejor toma de decisiones de los industriales interesados en reducir los problemas de los engranes rectos normalizados como ruido, desgaste abrasivo, desgaste adhesivo, temperatura y esfuerzos inducidos por la relación de sobreposición entre dientes acoplados; proponiéndoles una solución práctica que abrirá nuevas vías de investigación.

Ruido, Temperatura, Abrasión

Citation: JIMÉNEZ-RABIELA, Homero, VÁZQUEZ-GONZÁLEZ, Benjamín, RAMÍREZ-CRUZ, José Luis and BRAVO-ACOSTA, Adrian Gustavo. Spur gears with contact ratio less than unity. Journal Innovative Design. 2022, 6-15: 26-34

*Correspondence to the Author (e-mail: hjr@azc.uam.mx)
† Researcher contributing as first author.

Introduction

The movement transmission mechanism through spur gears, as well as the corresponding induced efforts, have aroused the interest of the scientific community. Contact relationship has been considered a critical factor for the qualitative and quantitative evaluation of the general behaviour of such gears.

Due to the importance of the subject, Díaz González, D. J. (2022) designed and manufactured a transportation vehicle for people with limited mobility by implementing Theo Jansen mechanism proportions and a mechanical transmission.

Badel Iriarte, A. A. (2022) Improved and characterized a pinion pump test bench for viscous fluids.

Cleveland Poo, B. (2022) Studed the torsional and radial vibrations of a spur gear transmission.

Nunura Dávila, L. A. (2022) designed and simulated a mechanical ventilator to treat respiratory failure in critical care for adults in Lambayeque.

Barroso-Molero, J. M. (2022) designed a speed reducer for a conveyor belt industrial.

ANSI/AGMA 1010-F14 (2020) Standard. Appearance of Gear Teeth – Terminology of Wear and Failure. Identifies and describes the classes of common gear failures and illustrates their degrees deterioration.

AGMA Standard 915-1-A02. Inspection Practices – Part 1: Cylindrical Gears – Tangential Measurements. It provides a Code of Practice dealing with the relevant inspection of the tangential component and runouts of gears (measurements referred to single flank contact). Supplement to ANSI/AGMA 2015-1-A01. ISBN: 1-55589-798-3.

On the page https://vsip.info/cap-10-modos-de-falla-comunes-en-engranajes-pdf-free.html the most common failure modes in gears are described, stating that the cracking of the teeth can initiate on the face and spread to the opposite flank.

Maras, S. *et al*. (2021) used vibration analysis and statistical process control to analyse failures in spur gears.

El Anouar, B. A. *et al*. (2016) they studied tooth wear on helical gears and stated: Vibration analyses in the time and frequency domain will enable wear diagnosis.

Herrera, A. *et al.* (2015) presented a study base on monitoring for early detection of possible tooth breakage in spur gears.

Pleguezuelos, M. & Pedrero, J. I. (2009) studied the performance of conventional spur gears, with non-uniform load distribution and variable friction along the line of action.

Regarding a pair of gears with contact ratio greater than unity an analogous pair with said ratio less than unity; eliminates the possibility of overlapping; reduces the number of impacts between teeth, noise, system temperature, abrasive wear, and adhesive wear.

Additional to the added value indicated in the previous paragraph; the pair of gears with a contact ratio less than unity also makes it possible to reduce the time of application of the load that generates efforts and work, the plastic deformation, the removal of material, the rolling of the profile, the grooves parallel to the direction of slip, wear in the support areas of the gears on their axes, the variation in the distance between centres, the radial pressure, the transverse vibrations of the entire rotor system. All the above with a considerable decrease in the efforts due to bending in the teeth; since decreasing their number increases their width, increases to the cube the moment of inertia, and decreases the bending effort.

Base on the assumption that it is always possible to optimize the interface between two components of a system, the proposed reduction of the contact ratio solves the problem caused by abrasive and adhesive wear. In the second section, the parameters, their units, and functional relationships between them are defined. A pair of gears with a standard number of teeth is described in the third section. The fourth section describes the pair of gears with a reduced number of teeth compared to the normalized one. The results are presented, analysed, and compared in the fifth, sixth and seventh sections.

ISSN-2523-6830

Nomenclature

The meanings of some variables are shown in Figures 1, 2 and 3, all of them are explained below. P_d = 4 = diametral pitch in teeth per inch of pitch diameter; $P_{c1} = P_{c2}$ = circular pitch in inches, in gears 1 or 2; $P_{c3} = P_{c4}$ = circular pitch in inches, in gears 3 or 4; $P_{b1} = P_{b2}$ = base pitch in inches, in gears 1 or 2; $P_{b3} = P_{b4}$ = base pitch in inches, in gears 3 or 4; N_i with $i = 1, 2, 3, 4$ = number of teeth in gear i; $r_1 = r_3$ = 2.5 = pitch radius in inches, on gears 1 or 3; $r_2 = r_4$ = 3.75 = pitch radius in inches, on gears 2 or 4; $r_{a1} = r_{a3}$ = addendum radius in inches, on gears 1 or 3 = $r_1 + \frac{1}{P_d} = r_3 + \frac{1}{P_d}$; $r_{a2} = r_{a4}$ = addendum radius in inches, on gears 2 or 4 = $r_2 + \frac{1}{P_d} = r_4 + \frac{1}{P_d}$; φ = 25 = pressure angle in degrees; $r_{b1} = r_{b3}$ = base radius in inches, on gears 1 or 3 = $r_1 cos\varphi = r_3 cos\varphi$; $r_{b2} = r_{b4}$ = base radius in inches, on gears 2 or 4 = $r_2 cos\varphi = r_4 cos\varphi$. α_i = angle subtended by half a tooth on the pitch circumference in degrees, in gear i = $\frac{90°}{N_i} - \frac{0.2}{P_d}$; β_i = angle subtended by half a gap on the pitch circumference in degrees, in gear i = $\frac{90°}{N_i} + \frac{0.2}{P_d}$. $\omega_1 = \omega_3$ = angular velocity in radians per second clockwise, on gears 1 or 3 = $1.5\omega_2 = 1.5\omega_4$; $\omega_2 = \omega_4$ = angular velocity in radians per second counter clockwise, on gears 2 or 4. Of the pair of teeth to monitor A, B, C, D, E, G are loci on the pressure line; A is the tangency with the base circumference of gears 1 or 3; B is the start of contact and is also the intersection with the addendum circumference of gears 2 or 4; C is the flank tangency at 1 with face at 2; D is the tangency of the pitch circumferences of gears 1 and 2 and also the tangency of the pitch circumferences of gears 3 and 4; E is the tangency of face at 1 with flank at 2; G is the end of the contact and is also the intersection with the addendum circumference of gears 2 or 4; z = distance from B to G; $O_1 = O_3$ = geometric centre of gears 1 or 3; $O_2 = O_4$ = geometric centre of gears 2 or 4; R_j with j = A, B, C, D, E, G, H is the position vector j, with respect to O_1 or O_3; $R_{jO2} = R_{jO4}$ is the position vector j, with respect to O_2 or O_4; B, C, D, E and G with subscript 1 or 2 are the material contact lines, on gears 1 or 2, at loci B, C, D, E and G.

R_v = speed ratio = $\frac{\omega_{1,3}}{\omega_{2,4}} = 1.5$; R_c = contact ratio = $\frac{z}{P_{bi}}$; σ_{max} = maximum Von Mises effort in pounds per square inch; F = force in pounds; T = torque in inch pounds; t = time in seconds for the pair of teeth to be monitored to pass their initial contact to their final contact; σ_{ta} = effort for tolerances and adjustments = effort due to mechanical errors.

Figure 1 corresponds to the initial contact of the teeth to be monitored. Figure 2 corresponds to the final contact of the teeth to be monitored. From Figures 1 and 2 the distance from B to E equals the distance from C to G.

Figure 3 shows the material lines at the teeth to be monitored, which contact at the corresponding loci on the pressure line at locus B.

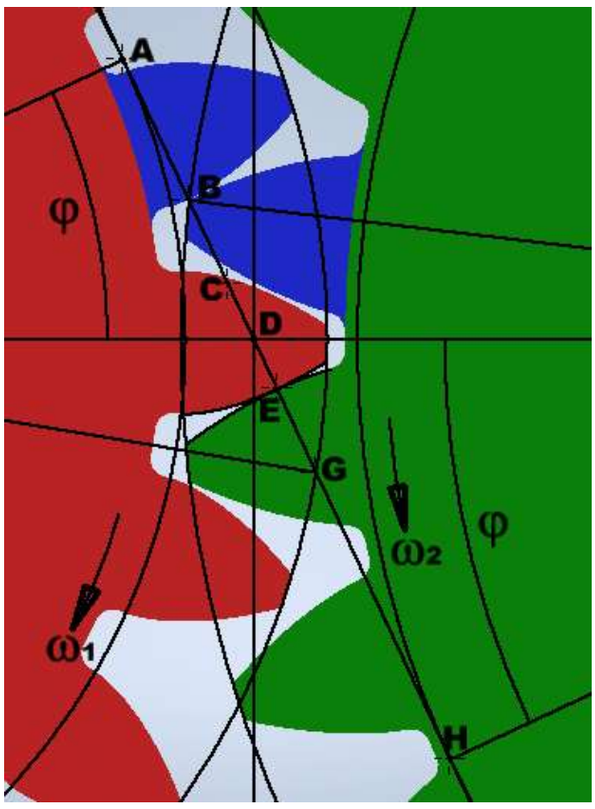

Figure 1 Contact on B
Own Elaboration

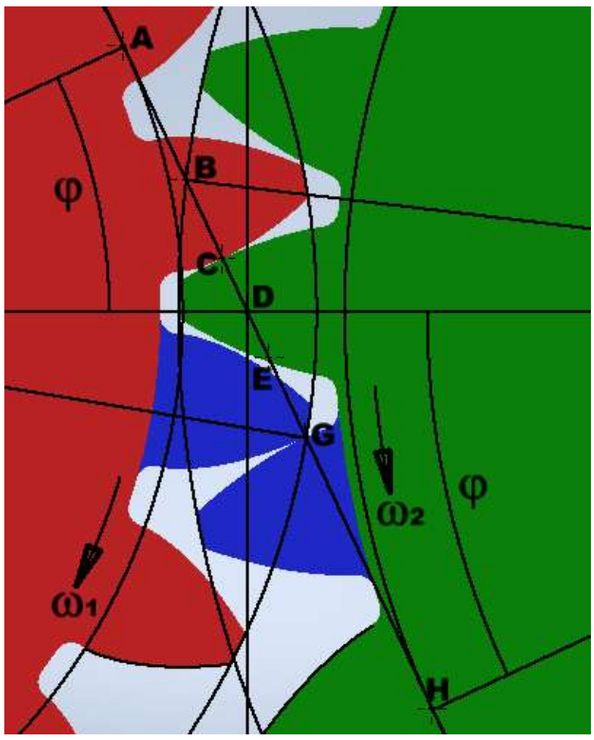

Figure 2 Contact on G
Own Elaboration

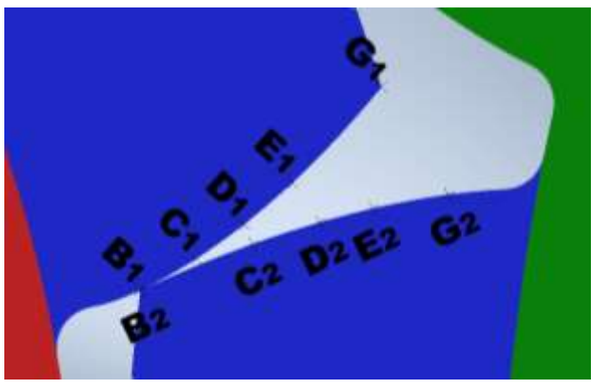

Figure 3 Material lines
Own Elaboration

Pair of Gears with Standard Number of Teeth

It is formed by gears 1 and 2, with 20 and 30 teeth respectively. From Figure 1 or 3, the distance from B to G from the beginning to the end of the contact of the gears to be monitored, is equal to:

$$z = \overline{AG} + \overline{BH} - \overline{AD} - \overline{DH} \quad (1)$$

$$\overline{AG} = \sqrt{(r_{a1})^2 - (r_{b1})^2} \quad (2)$$

$$\overline{BH} = \sqrt{(r_{a2})^2 - (r_{b2})^2} \quad (3)$$

$$\overline{AD} = r_1 sen\varphi \quad (4)$$

$$\overline{DH} = r_2 sen\varphi \quad (5)$$

Dividing z between P_{bi} we obtain:

$$R_c = \frac{zN_1}{2\pi r_1 cos\varphi} = \frac{zN_2}{2\pi r_2 cos\varphi} \quad (6)$$

Making equations of the of addendum circumference of gears 1 and 2 simultaneous with the equation of the pressure line, we obtain:

$$y_B = \overline{BH} cos\varphi - r_2 sen\varphi cos\varphi \quad (7)$$

$$x_B = r_1 - \overline{BH} sen\varphi + r_2 (sen\varphi)^2 \quad (8)$$

$$y_G = cos\varphi (r_1 sen\varphi - \overline{AG}) \quad (9)$$

$$x_G = r_1 + \overline{AG} sen\varphi - r_1 (sen\varphi)^2 \quad (10)$$

Equations (7) to (10) will be used to obtain the magnitude, direction, sense and point of application of the corresponding position vectors.

The distance from B to G divided between distance from B to E is equal to the contact ratio, this condition was used to define the position vector of point E.

If the graphic, structural and mechanical errors for both gears are zero and the contact ratio is greater than unity and less than 2; of the time t a percentage will correspond to contact between two pair of teeth and another to contact between a pair of teeth. During that same time t there will be 2 impacts between the teeth of gears 1 and 2.

Of the contact between two pairs of teeth; according to Figure 1, be first the one that does it in B and second the one that does it in E. If the graphic and structural errors are zero in both gears, with mechanical errors equal to zero for gear 1 and with mechanical errors different from zero for gear 2; takings as reference the two teeth of the first and tooth of gear 1 of the second, the following scenarios can be generated.

a) The separation of the teeth of gear 2 is greater than the design, the contact of the second pair of teeth, in the position shown in Figure 4, will be impossible and the energy will be transmitted only through the first pair.

ISSN-2523-6830

A contact ratio greater than unity in theory cannot be guaranteed in practice. It should not be overlooked that the second pair of teeth will contact each other for a short time prior to the initial contact of the first pair of teeth.

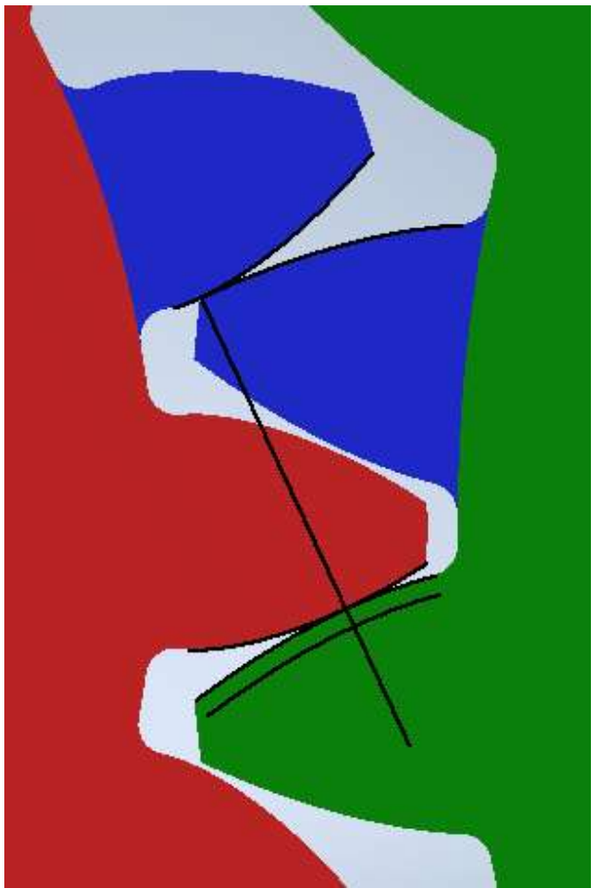

Figure 4 Contact only in B
Own Elaboration

With force F_B equal to 200 and T equal to 453.1538935183, the maximum von Mises stress equal to 20010 was determined using the finite element method, see Figures 5 and 6.

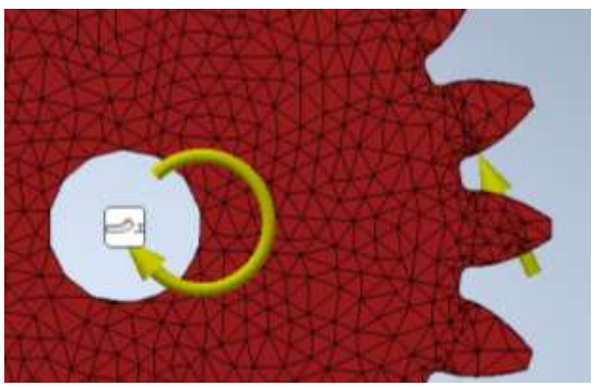

Figure 5 Meshed 1,2
Own Elaboration

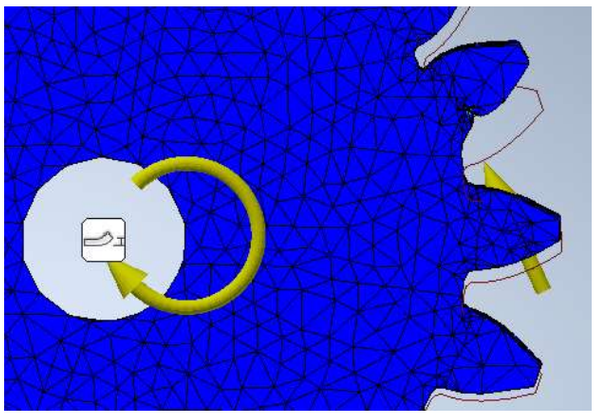

Figure 6 Numerical simulation 1,2
Own Elaboration

b) The separation of the teeth of gear 2 is equal to the of design, the contact of the second pair of teeth will be possible and the energy will be transmitted through the two pair of teeth, see Figure 7. Note that the contact in B will be more efficient than in E, because the radial component is smaller. Considering the mechanical errors in gear 2 with their tolerances and fits, the probability of this scenario is minimal.

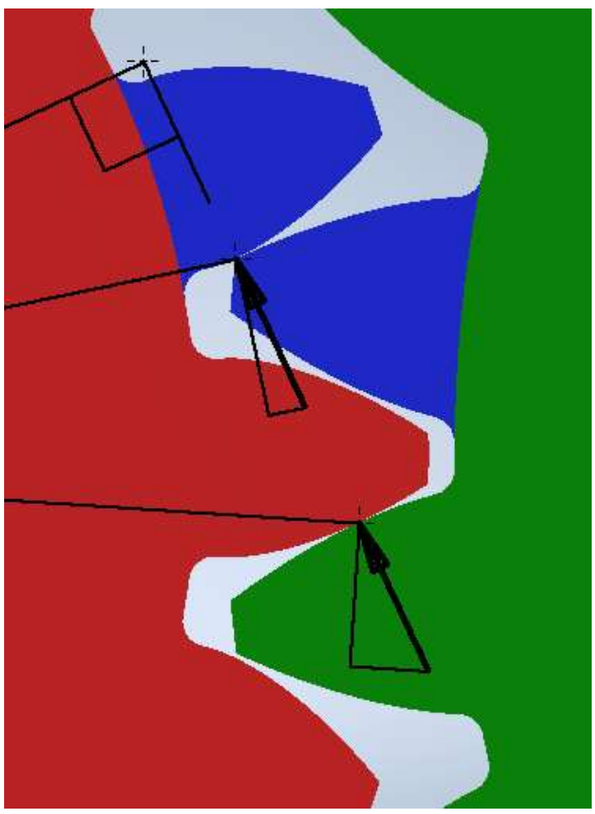

Figure 7 Contact in B and E
Own Elaboration

ISSN-2523-6830

With force F_B equal to 100, force F_E equal to 100 and T equal a 453.1538935183, the maximum von Mises stress equal to 10020 was determined using the finite element method.

c) The separation of the teeth of gear 2 is less than the of design, there will be contact between the first and the second pair of teeth, see Figure 8. When the teeth of gear 2 engage with the teeth of gear 1; the scenario b will be generated; also forces caused by the mechanical errors of gear 2 will be generated which are not shown due to their random nature, which oppose the work for which the system was designed. The contact efforts induce energy losses, those and these will increase for gear teeth separation minor.

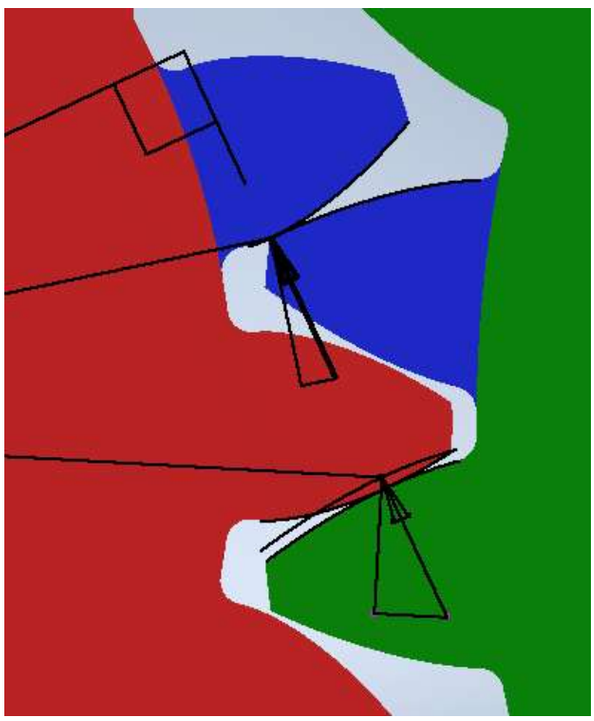

Figure 8 Abrasion and adhesion
Own Elaboration

The forces shown in Figures 5 through 8 are on gear teeth 1 and collinear with the line of pressure.

Pair of Gears with Smaller Number of Teeth

This pair of gears, 3 and 4, have 12 and 18 teeth respectively to keep the velocity ratio constant. Since z is the distance between locus B and G, It can be calculated with (1).

Dividing z between P_{bi} we obtain:

$$R_c = \frac{zN_3}{2\pi r_3 cos\varphi} = \frac{zN_4}{2\pi r_4 cos\varphi} \quad (11)$$

Making the equations of the of addendum circumference of gears 3 and 4 simultaneous with the equation of the line of pressure, analogous equations to (7) to (10) are obtained.

The position vectors of A, B, D, G and H are invariant with respect to those defined in the pair of gears 1 and 2.

Since the contact of the first pair of teeth will have ended when initiate contact the second, the position vectors of C and E will not exist.

For this pair of gears, the contact ratio is less than unity and, therefore, there will be contact between only one pair of teeth, see Figure 9.

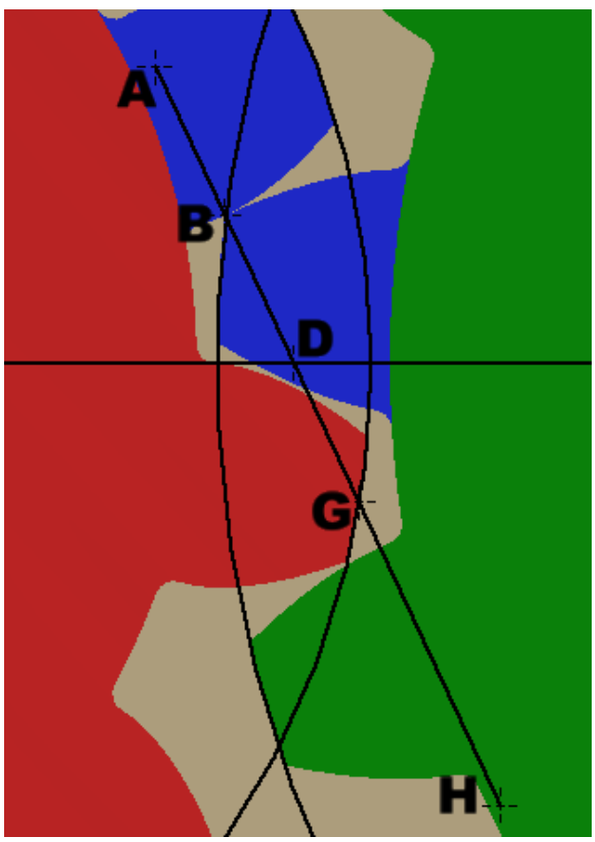

Figure 9 Initial contact between 3 and 4
Own Elaboration

The action and reaction forces along the pressure line will generate effort and work. When tooth 4 engages with tooth 3, the forces will correspond to direct contact along the pressure line or rolling contact at D.

Energy losses will be lower. When the number of teeth decreased, the angle subtended by a tooth increase; consequently, the moment of inertia increases to the cube due to the increase in width, therefore decrease the efforts induced by a load. Prior to the beginning of the contact between a pair of teeth and having finished the contact of the pair of teeth that goes ahead, there will be a short time without contact between the teeth, which will not imply that the system no longer works. During time t there will be only one pair of teeth in contact and only one impact.

With force at B equal to 200 and torque equal to 453.1538935183, the maximum Von Mises stress equal to 19100 was determined using the finite element method; see Figures 10 and 11.

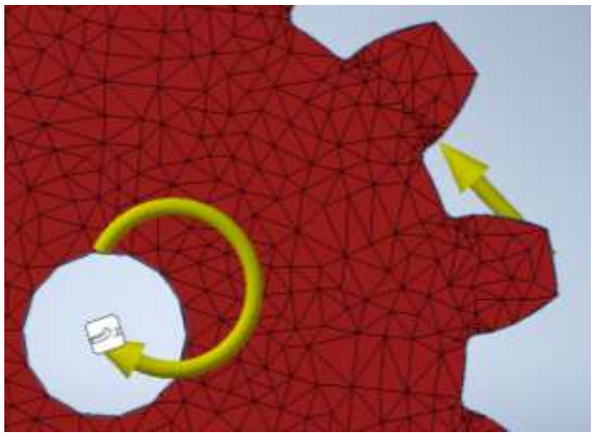

Figure 10 Meshed 3,4
Own Elaboration

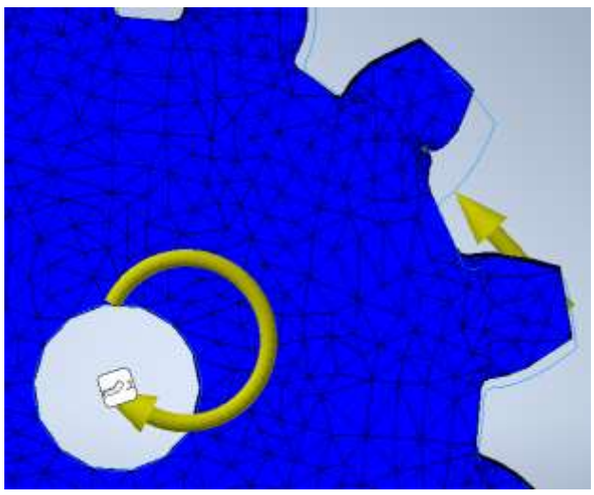

Figure 11 Numerical simulation 3,4
Own Elaboration

Results

The input data of the two systems are indicated in Table 1.

i	1	2	3	4
P_d	4	4	4	4
φ	25	25	25	25
r_i	2.5	3.75	2.5	3.75
N_i	20	30	12	18

Table 1 Gears data
Own Elaboration

The numbers of teeth on the gears are such that the same speeds ratio between 1,2 and 3,4 is preserved.

For better comparison, the contact ratio for 1,2 and 3,4 are listed in Table 2.

i	1	2	3	4
z	1.026393766		1.026393766	
P_{bi}	0.7118124714		1.186354119	
R_c	1.4419440614		0.8651664368	

Table 2 Contact ratios
Own Elaboration

The maximum von Mises stress are recorded in Table 3.

Scenary	σ_{max} at 1	σ_{max} at 3
A	20010	----------
B	10020	----------
C	10020 + σ_{ta}	----------
unique	----------	19100

Table 3 Efforts maximum
Own Elaboration

Table 4 shown distances between loci, see Figures 1 and 2, as well as vectors of position of input and output teeth, see Figure 3.

Distance	In 1	In 3
BE	0.7118124714	----------
BC = EG	0.3145812946	----------
R_B	2.3274025727	2.3274025727
R_G	2.75	2.75
R_E	2.5847511397	----------
R_{CO2}	3.8434188264	----------
R_{EO2}	3.6747549369	----------
R_{GO2}	3.5670068543	3.5670068543

Table 4 Distances
Own Elaboration

ISSN-2523-6830

Analysis of Results

In gear pair 1 and 2, for 30.6491821169 percent of t there are two pairs of teeth in contact and for 69.3508178831 percent the contact is between a unique pair of teeth. During the same time t there Will be two couplings (shocks) between the teeth of both gears.

In the pair of gears 3 and 4, during 100 percent of t there is a pair of teeth in contact. During 13.48335632 percent of t there are no teeth in contact. During 113.48335632 percent of t there will be a coupling (shock) between of both gears.

Results Comparison

From the results obtained for the pair of gears with normalized number of teeth (20 and 30), and for the pair of gears with reduced number of teeth (12 and 18), it can be asserted:

For a contact ratio equal to 1; when any pair of teeth begins their contact, the pair of teeth ahead will be ending their contact; the loads will act, in any pair of teeth, on the tip of the tooth of gear 2 and on the flank of the tooth of gear 1; the loads will act, in the pair of teeth ahead, on the tip of the tooth of gear 1 and on the flank of the tooth of gear 2. Mechanical errors in the gears make it impossible, in practice, to obtain the unity contact ratio. Contact ratio greater or less than unity? is the logical question.

To answers it, it is necessary to consider that currently the contact ratios of spur gears are greater than unity and have the following disadvantages: abrasive wear, adhesive wear, pitting, variable distance between centre, noise, high temperatures, among others; all of them caused by mechanical errors.

For contact ratios less than unity. Even with mechanical errors, the disadvantages mentioned in the previous paragraph will be considerably minors. It will always be more convenient, considering tolerances and fits, to engage one pair of teeth than to engage two pairs of teeth. By reducing the number of teeth, the circular pitch increases, increasing the width of the tooth as a cantilever beam, reducing consequently the efforts at the root of the tooth.

Even when the presented case study modifies the normalizes number of teeth (20 and 30) reducing it to (12 and 18), it is possible to reduced it to 10 and 15, 8 and 12, 6 and 9; if the passage of one tooth of each gear at a time is ensured.

Gratitude

The authors are grateful for the institutional support of the Universidad Autónoma Metropolitana, the Azcapotzalco Campus, the Division of Basic Sciences and Engineering, and the Department of Energy.

Financing

This work has been financed by the Department of Energy.

Conclusions

The proposed spur gear pair design will reduce temperature, noise, abrasive wear, adhesive wear, and pitting, contributing to more sustainable industrial processes. The present work does not significantly modify the possibility of interference between teeth of the pair of spur gear, constituting a niche of opportunity to improve the behaviour of the system.

Referencies

ANSI/AGMA. (2020). *AGMA 915-1-A02*. American Gear Manufacturers Association (AGMA): ANSI/AGMA.

ANSI/AGMA. (2020). *ANSI/AGMA 1010-F14*. American Gear Manufacturers Association (AGMA): ANSI/AGMA.

Badel Iriarte, A. A.. (2022). *Mejora y caracterización de banco de pruebas y bomba de piñones para fluidos viscosos*. agosto 14, 2022, de Universidad de Antioquia Sitio web: https://hdl.handle.net/10495/26244

Barroso-Molero, J. M. (2022). *Diseño de una reductora de velocidad para cinta transportadora industrial*. Universidad de Jaén, Escuela Politécnica Superior de Linares: Universidad de Jaén.

Cleveland Poo, B.. (2022). *Estudio teórico de las vibraciones torsionales y radiales de una transmisión de engranajes rectos*. Universidad de Concepción, Facultad de Ingeniería, Departamento de Ingeniería Mecánica: Universidad de Concepción.

Díaz González, D. J. (junio 14, 2022). *Diseño y manufactura de vehículo de transporte para personas con movilidad limitada implementando las proporciones de mecanismos de Theo Jansen y una transmisión mecánica*. agosto 14, 2022, de Universidad de los Andes, Facultad de Ingeniería, Departamento de Ingeniería Mecánica Sitio web: http://hdl.handle.net/1992/57961

El Anouar, B. A., Elamrani, M., Elkihel, B. & Delaunois,, F.. (marzo 27, 2019). *Surveillance et Détection des défauts d´engregages par analyse vibratoire*. agosto 14, 2022, de Conference 3éme édition du Colloque international sur le monitoring des systémes industriels (CIMSI) At Fés URL: https://www.researchgate.net/publication/320624084_Surveillance_et_detection_des_defauts_d%627engrenages_par_analyse_vibratoire

Herrera, A., Jaimes, I., & Quiroga, J.. (noviembre 24, 2015). *Estudio experimental de fallas en engranajes rectos por desalineación, excentricidad y diente roto*. agosto 14, 2022, de Universidad Industrial de Santander. Escuela de Ingeniería Mecánica. DOI: https://doi.org/10.14482/inde.34.1.7945 URL: redalyc.org/journal/852/85244549001/html/

MaraS, S., Arslan, H., & Birgören, B.. (julio 06, 2021). *Detection of Gear Wear and Falts in Spur Gear System Using Statistical Parameters and Univariate Statistical Process Control Charts*. agosto 13, 2022, de Arabian Journal for Science and Engineering https://doi.org/10.1007/s13369-021-05930-y RESEARCH ARTICLE-MECHANICAL ENGINEERING URL: https://www.researchgate.net/publication/353002857_Detection_of_Gear_Wear_and_Faults_in_Spur_Gear_Systems_Using_Statistical_Parameters_and_Univariate_Statistical_Process_Control_Charts

Nunura Dávila, L. A. (2022). *Diseño y simulación de ventilador mecánico para tratar insuficiencia respiratoria en cuidados críticos de adultos en Lambayeque*. agosto 14, 2022, de Universidad Nacional Pedro Ruiz Gallo Sitio web: https://hdl.handle.net.20.500.12893/10113

PLEGUEZUELOS, M., & PEDRERO, J. I.. (2009, enero 12). MODELO ANALÍTICO DE RENDIMIENTO DE ENGRANAJES RECTOS CONVENCIONALES. Revista Interamericana de Ingeniería Mecánica. ISSN: 1137-2729. URL: http://creativecommons.org/licences/by-nc-nd/4.0, agosto 14, 2022, 13, No. 1, pp. 27-38.

vsip. (2022). *10. Modos de falla comunes en engranajes*. agosto 14, 2022, de vsip Sitio web: https://vsip.info/cap-10-modos-de-falla-comunes-en-engranajes-pdf-free.html

ISSN-2523-6830

[Title in Times New Roman and Bold No. 14 in English and Spanish]

Surname (IN UPPERCASE), Name 1st Author†*, Surname (IN UPPERCASE), Name 1st Coauthor, Surname (IN UPPERCASE), Name 2nd Coauthor and Surname (IN UPPERCASE), Name 3rd Coauthor

Institutional Affiliation of Author including Dependency (No.10 Times New Roman and Italic)

International Identification of Science - Technology and Innovation

ID 1st Author: (ORC ID - Researcher ID Thomson, arXiv Author ID - PubMed Author ID - Open ID) and CVU 1st author: (Scholar-PNPC or SNI-CONACYT) (No.10 Times New Roman)

ID 1st Coauthor: (ORC ID - Researcher ID Thomson, arXiv Author ID - PubMed Author ID - Open ID) and CVU 1st coauthor: (Scholar or SNI) (No.10 Times New Roman)

ID 2nd Coauthor: (ORC ID - Researcher ID Thomson, arXiv Author ID - PubMed Author ID - Open ID) and CVU 2nd coauthor: (Scholar or SNI) (No.10 Times New Roman)

ID 3rd Coauthor: (ORC ID - Researcher ID Thomson, arXiv Author ID - PubMed Author ID - Open ID) and CVU 3rd coauthor: (Scholar or SNI) (No.10 Times New Roman)

(Report Submission Date: Month, Day, and Year); Accepted (Insert date of Acceptance: Use Only ECORFAN)

Abstract (In English, 150-200 words)

Objectives
Methodology
Contribution

Abstract (In Spanish, 150-200 words)

Objectives
Methodology
Contribution

Keywords (In English)

Indicate 3 keywords in Times New Roman and Bold No. 10

Keywords (In Spanish)

Indicate 3 keywords in Times New Roman and Bold No. 10

Citation: Surname (IN UPPERCASE), Name 1st Author, Surname (IN UPPERCASE), Name 1st Coauthor, Surname (IN UPPERCASE), Name 2nd Coauthor and Surname (IN UPPERCASE), Name 3rd Coauthor. Paper Title. Journal Innovative Design. Year 1-1: 1-11 [Times New Roman No.10]

* Correspondence to Author (example@example.org)
† Researcher contributing as first author.

Introduction

Text in Times New Roman No.12, single space.

General explanation of the subject and explain why it is important.

What is your added value with respect to other techniques?

Clearly focus each of its features

Clearly explain the problem to be solved and the central hypothesis.

Explanation of sections Article.

Development of headings and subheadings of the article with subsequent numbers

[Title No.12 in Times New Roman, single spaced and bold]

Products in development No.12 Times New Roman, single spaced.

Including graphs, figures and tables-Editable

In the article content any graphic, table and figure should be editable formats that can change size, type and number of letter, for the purposes of edition, these must be high quality, not pixelated and should be noticeable even reducing image scale.

[Indicating the title at the bottom with No.10 and Times New Roman Bold]

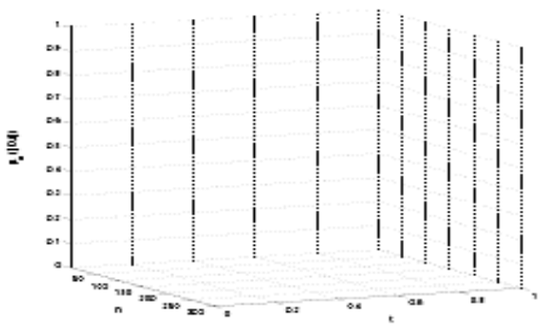

Graphic 1 Title and *Source (in italics)*

Should not be images-everything must be editable.

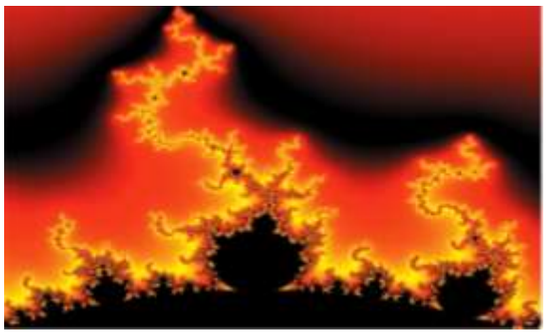

Figure 1 Title and *Source (in italics)*

Should not be images-everything must be editable.

Table 1 Title and *Source (in italics)*

Should not be images-everything must be editable.

Each article shall present separately in **3 folders**: a) Figures, b) Charts and c) Tables in .JPG format, indicating the number and sequential Bold Title.

For the use of equations, noted as follows:

$$Y_{ij} = \alpha + \sum_{h=1}^{r} \beta_h X_{hij} + u_j + e_{ij} \qquad (1)$$

Must be editable and number aligned on the right side.

Methodology

Develop give the meaning of the variables in linear writing and important is the comparison of the used criteria.

Results

The results shall be by section of the article.

Annexes

Tables and adequate sources

Thanks

Indicate if they were financed by any institution, University or company.

ISSN-2523-6830

Conclusions

Explain clearly the results and possibilities of improvement.

References

Use APA system. Should not be numbered, nor with bullets, however if necessary numbering will be because reference or mention is made somewhere in the Article.

Use Roman Alphabet, all references you have used must be in the Roman Alphabet, even if you have quoted an Article, book in any of the official languages of the United Nations (English, French, German, Chinese, Russian, Portuguese, Italian, Spanish, Arabic), you must write the reference in Roman script and not in any of the official languages.

Technical Specifications

Each article must submit your dates into a Word document (.docx):

Journal Name
Article title
Abstract
Keywords
Article sections, for example:

1. Introduction
2. Description of the method
3. Analysis from the regression demand curve
4. Results
5. Thanks
6. Conclusions
7. References

Author Name (s)
Email Correspondence to Author
References

Intellectual Property Requirements for editing:

- Authentic Signature in Color of Originality Format Author and Coauthors
- Authentic Signature in Color of the Acceptance Format of Author and Coauthors
- Authentic Signature in Color of the Conflict of Interest Format of Author and Co-authors.

ISSN-2523-6830

Reservation to Editorial Policy

Journal Innovative Design reserves the right to make editorial changes required to adapt the Articles to the Editorial Policy of the Research Journal. Once the Article is accepted in its final version, the Research Journal will send the author the proofs for review. ECORFAN® will only accept the correction of errata and errors or omissions arising from the editing process of the Research Journal, reserving in full the copyrights and content dissemination. No deletions, substitutions or additions that alter the formation of the Article will be accepted.

Code of Ethics - Good Practices and Declaration of Solution to Editorial Conflicts

Declaration of Originality and unpublished character of the Article, of Authors, on the obtaining of data and interpretation of results, Acknowledgments, Conflict of interests, Assignment of rights and Distribution.

The ECORFAN-Mexico, S.C Management claims to Authors of Articles that its content must be original, unpublished and of Scientific, Technological and Innovation content to be submitted for evaluation.

The Authors signing the Article must be the same that have contributed to its conception, realization and development, as well as obtaining the data, interpreting the results, drafting and reviewing it. The Corresponding Author of the proposed Article will request the form that follows.

Article title:

– The sending of an Article to Journal Innovative Design emanates the commitment of the author not to submit it simultaneously to the consideration of other series publications for it must complement the Format of Originality for its Article, unless it is rejected by the Arbitration Committee, it may be withdrawn.

– None of the data presented in this article has been plagiarized or invented. The original data are clearly distinguished from those already published. And it is known of the test in PLAGSCAN if a level of plagiarism is detected Positive will not proceed to arbitrate.

– References are cited on which the information contained in the Article is based, as well as theories and data from other previously published Articles.

– The authors sign the Format of Authorization for their Article to be disseminated by means that ECORFAN-Mexico, S.C. In its Holding Taiwan considers pertinent for disclosure and diffusion of its Article its Rights of Work.

– Consent has been obtained from those who have contributed unpublished data obtained through verbal or written communication, and such communication and Authorship are adequately identified.

– The Author and Co-Authors who sign this work have participated in its planning, design and execution, as well as in the interpretation of the results. They also critically reviewed the paper, approved its final version and agreed with its publication.

– No signature responsible for the work has been omitted and the criteria of Scientific Authorization are satisfied.

– The results of this Article have been interpreted objectively. Any results contrary to the point of view of those who sign are exposed and discussed in the Article.

Copyright and Access

The publication of this Article supposes the transfer of the copyright to ECORFAN-Mexico, SC in its Holding Taiwan for its Journal Innovative Design, which reserves the right to distribute on the Web the published version of the Article and the making available of the Article in This format supposes for its Authors the fulfilment of what is established in the Law of Science and Technology of the United Mexican States, regarding the obligation to allow access to the results of Scientific Research.

Article Title:

Name and Surnames of the Contact Author and the Coauthors	Signature
1.	
2.	
3.	
4.	

Principles of Ethics and Declaration of Solution to Editorial Conflicts

Editor Responsibilities

The Publisher undertakes to guarantee the confidentiality of the evaluation process, it may not disclose to the Arbitrators the identity of the Authors, nor may it reveal the identity of the Arbitrators at any time.

The Editor assumes the responsibility to properly inform the Author of the stage of the editorial process in which the text is sent, as well as the resolutions of Double-Blind Review.

The Editor should evaluate manuscripts and their intellectual content without distinction of race, gender, sexual orientation, religious beliefs, ethnicity, nationality, or the political philosophy of the Authors.

The Editor and his editing team of ECORFAN® Holdings will not disclose any information about Articles submitted to anyone other than the corresponding Author.

The Editor should make fair and impartial decisions and ensure a fair Double-Blind Review.

Responsibilities of the Editorial Board

The description of the peer review processes is made known by the Editorial Board in order that the Authors know what the evaluation criteria are and will always be willing to justify any controversy in the evaluation process. In case of Plagiarism Detection to the Article the Committee notifies the Authors for Violation to the Right of Scientific, Technological and Innovation Authorization.

Responsibilities of the Arbitration Committee

The Arbitrators undertake to notify about any unethical conduct by the Authors and to indicate all the information that may be reason to reject the publication of the Articles. In addition, they must undertake to keep confidential information related to the Articles they evaluate.

Any manuscript received for your arbitration must be treated as confidential, should not be displayed or discussed with other experts, except with the permission of the Editor.

The Arbitrators must be conducted objectively, any personal criticism of the Author is inappropriate.

The Arbitrators must express their points of view with clarity and with valid arguments that contribute to the Scientific, Technological and Innovation of the Author.

The Arbitrators should not evaluate manuscripts in which they have conflicts of interest and have been notified to the Editor before submitting the Article for Double-Blind Review.

Responsibilities of the Authors

Authors must guarantee that their articles are the product of their original work and that the data has been obtained ethically.

Authors must ensure that they have not been previously published or that they are not considered in another serial publication.

Authors must strictly follow the rules for the publication of Defined Articles by the Editorial Board.

The authors have requested that the text in all its forms be an unethical editorial behavior and is unacceptable, consequently, any manuscript that incurs in plagiarism is eliminated and not considered for publication.

Authors should cite publications that have been influential in the nature of the Article submitted to arbitration.

Information services

Indexation - Bases and Repositories

RESEARCH GATE (Germany)
GOOGLE SCHOLAR (Citation indices-Google)
MENDELEY (Bibliographic References Manager)
REDIB (Ibero-American Network of Innovation and Scientific Knowledge- CSIC)
HISPANA (Information and Bibliographic Orientation-Spain)

Publishing Services

Citation and Index Identification H
Management of Originality Format and Authorization
Testing Article with PLAGSCAN
Article Evaluation
Certificate of Double-Blind Review
Article Edition
Web layout
Indexing and Repository
ArticleTranslation
Article Publication
Certificate of Article
Service Billing

Editorial Policy and Management

69 Street. YongHe district, ZhongXin. Taipei-Taiwan. Phones: +52 1 55 6159 2296, +52 1 55 1260 0355, +52 1 55 6034 9181; Email: contact@ecorfan.org www.ecorfan.org

Journal Innovative Design

2523 6830
ISSN 2523-6830

www.ecorfan.org